From Mantle to Motzfeldt: A Genetic Model for Syenite-hosted Ta,Nb-mineralisation

Adrian A Finch[1,†], Jamie A McCreath[1], Callum DJ Reekie[1,*], William Hutchison[1], Abdulmalik Ismaila[1], Ashlyn Armour-Brown[2], Tom Andersen[3], Siri L Simonsen[3]

[1]School of Earth and Environmental Sciences, University of St Andrews, Irvine Building, St Andrews, Fife, KY16 9AL, UK.

[2]Angus and Ross plc, Kirkbymoorside, York, UK.

[3]Laboratory of Isotope Geology, Department of Geosciences, University of Oslo, Sem Sælands vei 1, Oslo, N-0316, NORWAY.

[†] Corresponding author, email: adrian.finch@st-andrews.ac.uk

**- now at: Department of Earth Sciences, University of Cambridge, Downing Street, Cambridge, CB2 3EQ, UK*

ABSTRACT

A genetic model for the Motzfeldt Tantalum-Niobium-rich syenite in south-west Greenland, considered to be one of the world's largest Ta prospects, is presented. The Motzfeldt primary magma formed early in regional Gardar (1273±6 Ma) rifting. Isotope signatures indicate that the Hf had multiple sources involving juvenile Gardar Hf mixed with older (Palaeoproterozoic or Archaean) Hf. We infer that other High Field Strength Elements (HFSE) similarly had multiple sources. The magma differentiated in the crust and ascended before emplacement at the regional unconformity between Ketilidian basement and Eriksfjord supracrustals. The HFSE-rich magmas crystallised Ta-rich pyrochlore which formed pyrochlore-rich crystal mushes, and it is these pyrochlore-rich horizons, rich in Ta and Nb, that are the focus of exploration. The roof zone chilled and repeated sheeting at the roof provided a complex suite of cross-cutting syenite variants, including pyrochlore microsyenite, in a 'Hot Sheeted Roof' model. The area was subject to hydrothermal alteration which recrystallized alkali feldspar to coarse perthite and modified the mafic minerals to hematite, creating the friable and striking pink-nature of the Motzfeldt Sø Centre. Carbon and oxygen isotope investigation of carbonate constrains fluid evolution and shows that carbonate is primarily mantle-derived but late-stage hydrothermal alteration moved the oxygen isotopes towards more positive values (up to 21 ‰). The hydrothermal fluid was exceptionally fluorine-rich and mobilised many elements including U and Pb but did not transport HFSE such as Ta, Hf and Nb. Although the U and Pb content of the pyrochlore was enhanced by the fluid, the HFSE contents remained unchanged and therefore Hf isotopes were unaffected by fluid interaction. While the effect on hydrothermal alteration on the visual appearance of the rock is striking, magmatic processes concentrated HFSE including Ta and the hydrothermal phase has not altered the grade. Exploration for HFSE mineralisation commonly relies on airborne radiometric surveying which is particularly sensitive to the presence of U, Th. A crucial lesson from Motzfeldt is that the best target is unaltered pyrochlore which was identified less easily by radiometric survey. Careful petrological/mineral studies are necessary before airborne survey data can be fully interpreted.

Keywords: pyrochlore, tantalum, alkaline, Gardar Province, hydrothermal alteration, Greenland

INTRODUCTION

High Field Strength Elements (HFSE), i.e. Ta, Nb, Hf and Zr, are transition metals that are the subject of global interest because of their uses in a wide variety of high-technology applications. Geopolitical controls on their supply mean that many are considered 'critical metals' (US Department of Energy 2011, British Geological Survey 2012, European Commission 2014) and Ta has attracted political attention for the role that columbite-tantalite ('coltan') mining may have played in conflict zones (Melcher *et al.* 2008, Mackay & Simandl 2014). Exploration for HFSE metals continues worldwide and is of great commercial and political interest. Most of the world's niobium is mined as pyrochlore from carbonatite, whereas tantalum is mined predominantly from peraluminous granitoid pegmatites as columbite-tantalite group minerals $(Fe,Mn)Ta_2O_5$ (see e.g. Melcher *et al.* 2015).

It has been known for many years that Nb and Ta are enriched in the Motzfeldt Complex, Gardar Province, South Greenland (e.g. Armour-Brown *et al.* 1983). In contrast to granite and granitoid-pegmatite paragenesis, HFSE at Motzfeldt are hosted within pyrochlore-rich syenite (McCreath *et al.* 2013) and, as yet, no petrogenetic model for this type of mineralisation has been described. The present paper is a description of petrology and petrogenesis of the North and North-Eastern margins of the Motzfeldt Centre, exploring the sources of high-field strength elements (HFSE) and the nature of the Nb and Ta-rich enrichment in the rocks. The present paper builds on extensive fieldwork (providing insights into regional structure), published geochemical data on the biotite (Finch 1995, Finch *et al.* 1995), zircon (McCreath *et al.* 2012) and pyrochlore (McCreath *et al.* 2013) at Motzfeldt and presents new data on the Lu-Hf isotopic analysis of zircon, F content in biotite mica and carbon and oxygen stable isotopes in carbonate. Lu-Hf isotopic analysis of zircon provides insights into the sources of the HFSE in the Motzfeldt magmas. F content in biotite mica constrains the F concentration in late-stage fluids and we use carbon and oxygen stable isotope data of carbonate to constrain fluid source. These novel data are integrated with published work to develop a genetic model for the formation of these syenite-hosted Nb,Ta-rich rocks.

GEOLOGICAL SETTING

The present study describes rocks of the 'Gardar Province', a term given to the products of intraplate alkaline magmatism associated with continental rifting in Mid-Proterozoic times. Gardar magmas intruded basement rocks (Fig .1), known the 'Julianehåb granite suite' (1900-1700 Ma) and part of the 'Ketilidian' orogeny, interpreted as an Andean continental margin (Chadwick & Garde 1996). These are calc-alkaline granitoids and granitoid-gneisses with varying degrees of

megacryst and fabric development alongside less frequent hornblende diorite, an association reminiscent of the 'appinite' suite of Scotland and Ireland (Allaart 1967). The Gardar Province post-dates the Ketilidian and represents the products of ***two*** periods of rift-related alkaline magmatism during the intervals ~1300-1270 Ma and 1180-1140 Ma, termed 'Early' and 'Late' Gardar respectively (Upton *et al.* 2003, Upton 2013). The earliest Gardar rocks preserved are sequences of interbedded clastic sediments and volcanic rocks referred to as the 'Eriksfjord formation'. These were formed as clastic sedimentation filled the rift as it subsided, interdigitated with the products of rift-related volcanism (lavas and pyroclastics). About 3 km thickness of these deposits is preserved (Poulsen, 1964). From *in situ* exposures and Eriksfjord xenoliths in Gardar central complexes, it is inferred that the Eriksfjord once covered much of SW Greenland. Andersen (2013) showed the depositional age of the Eriksfjord to be <1305 Ma. The extensional stress regimes active during the Gardar are inferred from the orientations of faults and dykes. In the early Gardar, tension was parallel to ENE-WSW and a series of NNW-SSE basic dykes resulted (Bartels *et al.* 2015). The Gardar Rift developed a series of central complexes, which represent fossilised magmatic systems. The Igaliko Complex, the largest association of igneous rocks within the Gardar Province, includes rocks of both Early and Late Gardar age (Upton *et al.* 2003), of which four regions (North Qôroq, Motzfeldt, North Motzfeldt and Narsarsuaq) are Early Gardar (Fig. 1). Radiometric chronology has been performed for several centres and is summarised in Table 1. Gardar magma reservoirs were formed within Ketilidian basement through a combination of block stoping, ring fracture and partial ring dyke formation (Emeleus & Harry 1970; Jones 1980). They represent fossilised subvolcanic systems and current exposure is estimated to be within a few km of the palaeo-land surface (Upton et al. 2003).

The Motzfeldt region, the focus of the present study, covers an area of approximately 150 km^2 with excellent 3-dimensional exposure in steep glacial valleys, dissected and partly surrounded by the Greenland inland ice (Fig. 1). The region is cut by major glaciers (particularly Qôroq glacier, in Greenlandic: Qoorqup sermia) and a lake (Motzfeldt Sø; Greenlandic: Motzfeldt-ip tasia). It includes Ketilidian basement rocks, Eriksfjord supracrustals and exhumed Gardar subvolcanic centres. Poulsen (1964) correlated the Eriksfjord sediments and volcanics in the Motzfeldt region with the Majût and Mussartût members to the SW, the lowest part of the Eriksfjord sequence. The primary geological feature of the Motzfeldt region is a series of steep-sided, elliptical, concentric igneous intrusions whose marginal contacts are vertical or dip slightly outwards. The rocks include syenite, nepheline syenite, syenogabbro and minor intrusives, ranging in composition from basic to evolved rocks; quartz normative to agpaitic (Emeleus & Harry 1970, Jones 1980, Tukiainen 1988, Schönenberger & Markl 2008).

The Motzfeldt region was mapped twice by the Geological Survey of Greenland and unfortunately each survey produced a different and largely contradictory nomenclature (cf. Emeleus & Harry 1970, Tukiainen 1988). This has created two parallel naming schemes, both of which continue to be used. The present article rationalises both schemes, integrating our own field studies, into a single coherent nomenclature (Appendix A), which is summarised below.

The earliest activity in Motzfeldt lies in the North and East. These rocks now include the Geologfjeld (GC), Motzfeldt Sø (MSC) and North Motzfeldt (NMC) Centres (Fig. 1), each of which comprises a nested series of syenite units. Younger activity, in the middle of the field area, cored out the older syenite and now comprises rocks in the middle, south and west of the complex. These include the Flinks Dal Centre (FDC) and the North Qôroq Centre (NQC) (Fig 1). An isolated syenite stock at Narsarsuaq (Narsarsuaq Centre, NC) sits to the west. The units within a centre are identified with a prefix (to denote the centre) and a rock description, such as 'MSC-Nepheline Syenite'. The youngest activity is a series of subhorizontal peralkaline sheets, and an arcuate monzonite dyke (locally known as 'larvikite') that likely represents a partial ring-dyke. The relative ages of these late-stage intrusives is not known, although they postdate other Motzfeldt magmatism. The sequence of Early Gardar events at Igaliko is inferred as: 1) GC, 2) MSC, 3) FDC, 4) NQC, 5) NMC, 6) peralkaline sheets, 7) monzonite ring dyke (Fig. 1).

During the Late Gardar, the rift adopted a dominant E-W sinistral transtension generating (or exploiting pre-existing) E-W faults and creating *en echelon* NE-SW dilation along which many Gardar dykes were intruded (Upton *et al.* 2003). The geography of Motzfeldt is now dominated by a deep NE-SW fjords and we infer that these exploit major vertical rift faults active in Late Gardar times. Two major syenite centres at South Qôroq and Igdlerfigssalik (modern spelling: Illerfissalik) are Late Gardar in age and the displacement of Late Gardar igneous rocks to the south (around South Qôroq, Emeleus & Harry 1970) show that movement on these E-W faults continued after magmatism ceased. The landscape is crossed by Late Gardar dykes (typically striking at 60°). A prominent alkali gabbro giant dyke crosses Motzfeldt at a 60° orientation and we infer it to be Late Gardar in age.

The present study focusses on the Early Gardar magmatism associated with the Motzfeldt Sø Centre (MSC). It is subdivided into: ***MSC – Marginal Arfvedsonite Syenite***, ***MSC – Altered Nepheline Syenite*** and ***MSC – Nepheline Syenite*** (Fig. 1). Within the MSC are a number of late microsyenite sheets termed the ***MSC – Peralkaline Microsyenite Suite***. Pervasive alteration within the Motzfeldt region is largely restricted to the MSC. Work by the Greenland and Denmark Geological Survey (GEUS, formerly GGU) (Tukiainen *et al.* 1984; Tukiainen 1988) in the MSC-Altered Nepheline Syenite revealed a number of localities with economically significant amounts of

Nb, Ta, Th, U, Zr and REEs hosted within pyrochlore supergroup minerals. These rocks, the host to Ta-rich pyrochlore (McCreath *et al.* 2013), and their genesis are the principal focus of this study.

Rocks of the Flinks Dal Centre (FDC, Emeleus & Harry 1970, Schönenberger & Markl 2008) are similar in composition to the MSC but they lack pervasive hydrothermal alteration. Tukiainen (1988) suggested that, whereas the MSC is exposed near the roof zone, FDC rocks are compositionally similar but exposed at a deeper level. The FDC is inferred to have avoided complex magmatic interactions between magma and roof and pervasive alteration concentrated in the roof zone. Comparison of the rocks of the FDC and MSC allow the influence of the hydrothermal alteration to be inferred.

MATERIALS AND METHODS

Fieldwork for the present study is the synthesis of several field seasons in the period 2001-2016, but we particularly draw upon data collected in 2005, 2006 and 2015. Fieldwork focussed on the areas to the N and E of Motzfeldt Sø and the samples in the present study derive from the MSC – Altered Nepheline Syenite unit in locations '1', '4', '5' and '6' (Fig. 1). The location numbers derive from target areas identified by Angus and Ross plc and all samples are in the collections of the University of St Andrews. Individual sample descriptions and locations (latitude and longitude) can be found in supplementary information and McCreath (2009).

Except where stated otherwise, the following analytical work was carried out in the School of Earth & Environmental Sciences at the University of St Andrews, UK. Rocks from the MSC and FDC were examined as polished thin sections or zircon separates, hand-picked under a binocular microscope and mounted on polished epoxy blocks. Electron microscopy and electron probe microanalyses (EPMA) on biotite were performed using a Jeol JXA 8200 Superprobe. A SAMx Energy Dispersive System (EDS) was used to obtain qualitative estimates of mineral compositions prior to quantitative analysis, particularly to ensure that all significant elements were present in WDS analytical programs. The electron beam operated at an accelerating voltage of 20 kV and a beam current of 30 nA. Data were processed using SAMx software with fully quantitative ZAF corrections to obtain final element analyses. The following well-characterised natural and synthetic standards were used during analyses: wollastonite (Ca), orthoclase (K), albite (Na, Al), quartz (Si), rutile (Ti), MgF_2 (F), metallic Fe, Mn. Back-scattered electron (BSE) images were acquired on the same instrument using an accelerating voltage of 15 kV with beam current of 20 nA to ensure a sharp image. Precision of compositional data to 95% confidence interval vary from element to element but are typically ~0.03 wt.%. In addition to the elements measured by WDS, biotite can

contain significant amounts of other ions, notably Li, Cl, Ba, Rb and Be (Bailey, 1984). During wavelength dispersive analysis (WDS), Cl, Rb and Ba were monitored using Energy Dispersive Spectral (EDS) analysis of the X-rays. Levels of these elements were below detection (~0.1 wt. %) and considered insignificant for the purposes of this investigation. Li and Be could not be determined using EDS but previous ion microprobe analyses of biotite from neighbouring Gardar centres show insignificant concentrations for both Li (1-25 ppm) and Be (<2 ppm) (Finch *et al.* 1995; Parsons *et al.* 1991).

C and O isotope analysis of powdered carbonate or whole-rock samples were performed using a Thermo Finnegan Delta plus XP continuous flow isotope ratio mass spectrometer attached to a Thermo Finnegan Gasbench II. Between 30 mg (but occasionally up to 1 g) of sample yielded sufficient CO_2 for isotope analysis. Samples were weighed on a microbalance and transferred to clean and dry borosilicate sample vessels and capped with a rubber septum, which retains an airtight seal after being punctured by a needle. The sample vessels are loaded into the GasBench II sample holder and are automatically flushed with He carrier gas. After the flush-fill process each sample is acidified with 100% anhydrous phosphoric(V) acid. The samples were left to react for a further 24 hr at 30˚C before automatic isotope analysis. Results are given in δ notation and expressed relative to Pee Dee Belemnite standard (PDB) for carbon and Standard Mean Ocean Water (SMOW) for oxygen in ‰. The internal precision measure is typically 0.01 – 0.03 ‰ for $\delta^{13}C$ and 0.01-0.03 ‰ for $\delta^{18}O$. The accuracy of the raw data is estimated using the NIST NBS-18 and NBS-19 standards. The external precision calculated using 10 standards give typical values of 0.01-0.04 ‰ for $\delta^{18}O$ and 0.01-0.02 ‰ for $\delta^{13}C$.

Qualitative EPMA mapping was performed on a Cameca SX-100 electron microprobe at the School of Geosciences at the University of Edinburgh, UK using wavelength dispersive spectrometers (WDS). Earlier carbon coating was removed using 0.25 µm diamond paste, followed by ultrasonic cleaning and a new carbon coating (20 nm). Images were acquired with an accelerating voltage of 20kV, 0.5 µm beam size and a residence time of 2 s per point. The crystal arrangement used to detect the elements of interest are: PET–Nb Lα; LLIF-Ta Lα; TAP-Na Kα. Data were acquired with the assistance of Dr Chris Hayward.

Lu-Hf isotopic analyses were carried out at the Laboratory of Isotope Geology, Mineralogical-Geological Museum, University of Oslo using a Nu Plasma HR mass spectrometer. Masses 172-179 were measured simultaneously in Faraday collectors. Ablation was conducted in helium at the following conditions: beam diameter 55 µm (aperture imaging mode); pulse frequency 5 Hz; beam fluence c. 2 J cm^{-2}, static ablation. Each ablation was preceded by a 30 s on-mass background measurement. The total Hf signal obtained was in the range 1.5-3.0 V. Under these conditions, 120-

150 s of ablation was required to obtain an internal precision of 0.000020 (1SE) (Heinonen *et al.* 2010). Isotope ratios were calculated using the Nu Plasma time-resolved analysis software. The raw data were corrected for mass discrimination using an exponential law, and the mass discrimination factor for Hf (fHf) was determined assuming $^{179}Hf/^{177}Hf = 0.7325$ (Patchett & Tatsumoto, 1980). Isobaric interferences were corrected using the algorithms of Elburg *et al.* (2013).

RESULTS

Field Analysis and Petrology

Geography. In the North and North-East of Motzfeldt, the focus of the present study, the highest points of the Motzfeldt region are flat table-top mountains (~1.6 km high) whose sides are deeply dissected by recent glaciation into steep valleys that cover >1.5 km of relief (Fig. 2a, b). This provides both a horizontal and vertical appreciation of the geology. The exposure is locally variable and many regions are covered by permanent ice, scree, glacial deposits and regolith. The central valleys are filled by boulders and gravels that form deposits up to several metres deep. Moraines are formed in corries and on plateaux. Trenches dug into the regolith on the higher ground show that it is dominated by mm-cm sized amphibole and feldspar sand and gravel but larger (<50 cm) blocks lie on the surface, providing a paved landscape in which blocks are within metres of their original positions, although blocks are lifted and rotated. Such landscapes superficially appear to be *in situ* exposure, and are recognised when dykes cut the region – the dykes appear coherent at distance (e.g. Fig. 2b) but on closer inspection are made up of rotated and shattered blocks scattered amongst the regolith. In such landscapes, bedrock geology can be inferred from the regolith. The vertical faces in the Motzfeldt region are striking (Fig. 2a,b) but deceptively unstable comprising unsupported chimneys and slabs. No sampling of these vertical faces was possible in the present study.

The mountains in the NE Motzfeldt region are strikingly flat, in contrast to the jagged mountains in the remainder of Southern Greenland. As we will see below, the geology of this area comprises a collapsed roof zone to a subvolcanic igneous centre. We infer that the table-top landscape results from recent glaciation in which the contact between igneous rocks and the Eriksfjord roof acted as a subhorizontal plane of weakness. Glaciation has therefore sliced along the roof zone itself and the geography of the mountain tops reflects to within a few 10s of metres the morphology of the top of the magma reservoir.

Field Geology. The study area comprises Ketilidian basement, rocks of the Eriksfjord Formation and Early Gardar syenites, all of which are cross-cut by late-Gardar dykes and faults (Fig. 1). The Eriksfjord Formation occurs *in situ* in the North and East of the region (Fig. 1) and commonly as rafts within later igneous rocks. It lies unconformably on the Ketilidian basement in the NE of the area. In the Motzfeldt region, Eriksfjord rocks are typically subhorizontal quartz arenite and quartz-rich conglomerates, often preserving cross-bedding and ripple marks. Units are dominated by quartz but some also contain clay and feldspar. The lavas are typically mafic-rich and are best observed in Locality 5 (N61° 11' 45.0" W044° 59' 39.5") showing well-preserved columnar jointing, pahoehoe flow textures, pillow structures and vesicular flow surfaces. Pyroclastic breccias are also observed. Aphyric and porphyritic trachyte (Finch et al., 2001) is also seen at the base of the sequence in this locality. Three diatremes cut the basement to the NE of Motzfeldt (Fig. 1). One diatreme (Fig. 1) contains Gardar carbonatite, gabbro and peridotite clasts with shattered Ketilidian basement, all of which are strongly hydrothermally altered such that feldspars in the gabbro and peridotite are strongly turbid and mafic minerals are altered to epidote and chlorite. The peridotites are interpreted as Early Gardar cumulates, i.e. olivine and pyroxene rich fractions of a gabbroic cumulate. The hydrothermal alteration indicates that the diatremes predate the igneous intrusions and therefore the clasts in the diatreme provide insights into magmatism preceding the preserved rocks of Motzfeldt age, and possibly those preserved below current exposure. No diatremes are seen cutting syenite in the Motzfeldt region.

The Eriksfjord and basement rocks are cut by Early Gardar magmatism. These are families of nested, cross-cutting subvolcanic centres (Fig. 1). The roof to the intrusion is preserved at Locality 4 in a spectacular vertical section through the roof zone (Fig. 2b) and Eriksfjord xenoliths, identical to rocks *in situ* nearby, are common. The MSC units (MSC - Nepheline Syenite, MSC - Altered Nepheline Syenite and MSC – Peralkaline Sheets, Fig. 1) are not rocks with a single mineralogy and texture, but are rather definable suites of complexly interdigitated syenite variants. MSC – Altered Nepheline Syenite, the host for much of the mineralisation, comprises strikingly orange or red syenite variants with alkali feldspar, sodic amphibole and/or pyroxene (Fig. 2c). The alkali feldspar is K-rich with substantial hematite staining, providing the strong red colour that characterises the MSC rocks in hand specimen. Amphibole forms black tabular crystals, whereas pyroxene is bright green, often as rosettes. Some syenite variants contain biotite laths, but in most the biotite overgrows opaques and is considered secondary in origin. Euhedral opaque oxides, members of the ilmenomagnetite solid solution, are widespread. Mafic minerals are often heavily altered to brown Fe oxides. Grain size varies over metre scales from exceptionally coarse syenite (>10 cm crystals) to microsyenite (1 mm crystals). Clearly defined chilled contacts are not observed. A series of late pegmatites form part of this unit, comprising quartz, alkali feldspar and

arfvedsonite, are notably rich in zircon and astrophyllite. These units provide the zircons for Lu-Hf isotopic analysis discussed below.

Pyrochlore is a common accessory in many Motzfeldt syenites, but the highest concentration is in a characteristic pyrochlore microsyenite facies within the MSC – Altered Nepheline Syenite. It typically occurs as fine euhedral to subhedral crystals disseminated throughout the rock or as rare pyrochlore-rich veinlets. Crystals occurring in the enriched veinlets are typically 100-300 μm, compared to an average of approximately 100 μm for the disseminated pyrochlore. Pyrochlore typically constitutes <15% of the rock, though in particularly enriched samples, it makes up ~25%. The pyrochlore microsyenite occurs in inclined sheets typically 10-20 cm wide without chilled contacts, a component of the late-magmatic sheeting that comprises the MSC-Altered Nepheline Syenite. The crystallisation sequences inferred from mineral textures are variable. Zircon, pyrochlore and opaques are usually euhedral and early formed. However some facies have euhedral alkali feldspar and interstitial mafics whereas in others the converse is true. Nevertheless all of the units with the MSC-Altered Nepheline Syenite are contemporaneous and part of a single magmatic episode. The pyrochlore microsyenite, the primary target for Ta and Nb, is widespread but laterally discontinuous; individual sheets cannot be mapped across terrain, nor correlated between drill cores. It contains predominantly (~80%) eu-to sub-hedral pink alkali feldspar crystals that are typically 1-3 mm in length, showing coarse perthite textures with an elongate tabular habit and strong mineral alignment. The modal amount of mafic minerals in the rock is typically <10%. The primary mafic mineral, usually amphibole, occurs interstitially but largely replaced by granular clusters of Fe-Ti oxide minerals and secondary micas.

Much, but not all, of the MSC-Altered Nepheline Syenite is intensely hydrothermally altered. The alteration is most obvious in outcrop as the reddening of alkali feldspar, the result of hematite formation along cleavage planes. All of the textural variants are equally altered. Feldspars are friable in hand specimen, intensely turbid in thin section and mafic minerals are replaced by knots of Fe oxides and mica. Dark biotite commonly overgrows ilmenomagnetite. Calcite and fluorite veining is also observed (Fig. 2d). At lower stratigraphic levels (e.g. the side of Motzfeldt Sø, ~50 m a.s.l.), the alteration is less well developed and the MSC – Nepheline syenite is a relatively homogeneous nepheline syenite. In addition, the pyrochlore microsyenite is less common at lower stratigraphic levels. On ascending a vertical section from the shore of Motzfeldt Sø up to the 1610 m summit, the degree of alteration increases, progressively more heterogeneity is observed and modal nepheline decreases.

MSC–Nepheline Syenite contains several large (100's m wide) rafts of basic rock (basalt) and arenite, identical to the Eriksfjord Formation rocks found to the North and East of Motzfeldt. These

are surrounded by nepheline syenite and are therefore xenoliths. In some regions (e.g. Location 4, Fig 1), characteristic textures in the xenoliths correspond to Eriksfjord rocks *in situ* nearby, demonstrating that the xenoliths have been transported no more than 10s of metres. The frequency of xenoliths increases going higher. It is observed that the Eriksfjord xenoliths preserved in the Motzfeldt magmatic rocks are dominated by lavas, whereas the Eriksfjord found *in situ* tends to be more commonly arenitic sediments.

The MSC – Peralkaline Sheets are a distinct, later series of inclined sheets, clearly visible in the NE side of Motzfeldt Sø and on the W side of Qooroq Fjord. These show less reddening of the feldspars, with white feldspar or nepheline and compositions varying from aegirine- and arfvedsonite-bearing microsyenite to microijolite (i.e. medium grained mesocratic rock comprising aegirine and nepheline). The frequency and thickness of peralkaline microsyenite sheets increase towards the higher stratigraphic levels.

EPMA

The major, minor and isotopic composition of zircon and pyrochlore from the FDC and MSC have been studied in detail elsewhere (McCreath *et al.* 2012, 2013) and hence have not been repeated in the present study. EPMA studies for the present study focus on pyrochlore and biotite. We analyse the same sections considered by McCreath et al. (2013). For pyrochlore, we identify grains which show chaotic zoning patterns under backscattered electron imaging. These chaotically zoned crystals were then mapped by EPMA to determine the spatial distribution of Na, Ta and Nb across the crystal. The results of a representative crystal are shown in Fig. 3. The BSE image of this crystal shows it to be a nm-scale intergrowth of multiple pyrochlore supergroup minerals. The distribution of the dark and light zones (representing variations in concentrations of heavy elements) indicate alteration around cracks and microfractures. EPMA maps, showing element distributions in the same crystal, are shown (Fig. 3). The Na distribution is chaotic, reflecting the Backscattered Electron Image. However the 'B'-site elements in pyrochlore, Ta and Nb, retain an oscillatory growth pattern.

Biotite mica is found throughout the rocks of the MSC – Altered Nepheline Syenite. The F content of mica is used as an indicator of the F activity of aqueous fluids associated with the emplacement of igneous bodies (Munoz 1984; Zhu & Sverjensky 1992; Finch 1995; Finch *et al.* 1995). Briefly the major element chemistry of biotite is determined at crystal growth, whereas the halogen content remains open to exchange down to low (e.g. <300 °C) temperatures (see Finch *et al.* 1995 for a fuller discussion). F in mica therefore reflects the F content of the late-stage fluid. We examine biotite from the MSC - Altered Nepheline Syenite and compare it with nepheline syenite

of the FDC to obtain insights into the relative F concentrations across the two units. Biotite is found throughout the MSC variant syenites in varying abundance from several small flakes per thin section to poikilitic phenocrysts (e.g. GJM06-31). Most commonly it forms irregularly shaped platelets growing intercumulus to pyroxene and amphibole (e.g. GJM06-63). In many samples small flakes of 'fringe biotite' grow in rims around small ilmenomagnetite accessory grains. Although 'fringe biotite' is often the most Fe-rich, we find no systematic difference between the other textural relationships of micas in their fluorine or major element chemistry.

A total of 128 electron microprobe analyses of 84 biotite crystals were made from texturally distinct variants of from the MSC - Altered Nepheline Syenite and 115 analyses of 62 biotite crystals from each major syenite facies in the FDC. Representative electron microprobe analyses are given in Table 2, including calculation of numbers of atoms per 22 oxygens and site allocations for all major elements. The complete dataset and site allocations are provided in supplementary data. In performing site allocations it is assumed that the tetrahedral site is always filled (8 atoms per 22 oxygen) by Si and then in turn by Al and Fe. Any excess Al or Fe is subsequently allocated to the octahedral site. The interlayer site is occupied by K, Ca or Na only.

The greatest variation in biotite from Motzfeldt comes from differences in the octahedral Fe and Mg content, relating to the annite-phlogopite solid solution. Variation within this solid-solution is expressed as atomic Fe/(Fe+Mg). Fe/(Fe+Mg) variation in MSC biotite is from 0.75 to annite (Fe/(Fe+Mg) = 1.0). The Fe/(Fe+Mg) content of biotite from the FDC spans a much larger range (0.25-0.95). The octahedral site totals vary between 5.1 and 5.8 in the MSC and 5.5 and 6.0 in the FDC indicating vacancies in the octahedral site from both formations. Vacancies may balance octahedral Ti^{4+}, by the exchange $2Mg^{2+} = Ti^{4+} + [vac]$.

Fluorine in biotite from the MSC – Altered Nepheline Syenite varies from below detection to 1.55 wt%, which relates to site occupancy up to 0.78 atoms per 22 O (total is 4). The F of biotite from the FDC covers a much larger range of lod-3.35 wt%, relating to fluorine up to 1.67 atoms per 22 O. The data from the FDC and MSC plot as distinct fields on the F vs Fe/(Fe+Mg) graph (Fig. 4). In both centres, F tends to increase with decreasing Fe/(Fe+Mg) and plots as a right-angled triangular field. This pattern is consistent with data from across the whole Gardar Province (Finch *et al.* 1995). Using the approach of Finch *et al.* (1995), a 'Maximum Fluorine Line', representing the hypotenuse of the right-angled triangular field, is added to each formation showing the maximum amount of F for a given Fe/(Fe+Mg) value. Such lines are used for qualitative comparison of different regions and do not represent thermodynamic functions.

C and O Isotopic Data

Carbonate minerals were identified using optical and cathodoluminescence (CL) petrography throughout the FDC and MSC. Calcite is the dominant carbonate, occurring in veinlets, disseminated grains and filling vugs. Carbonate minerals are sub-solidus alteration products, particularly associated with mafic minerals. Light Rare Earth Element (LREE)-bearing carbonate phases rich in Ce, La and Nd (tentatively identified as bastnäsite-(Ce), parisite-(Ce) or synchysite-(Ce)) and cancrinite are also identified (this work, Bradshaw 1988; Schönenberger & Markl 2008) in FDC and MSC rocks. Calcite carbonatite-rich clasts from the diatreme and a ferrocarbonatite (siderite) intrusive inclined sheet in the E of the area are also analysed.

Whole-rock samples from the FDC have $\delta^{13}C_{PDB}$ values of -3.80 to -6.61 ‰ with $\delta^{18}O_{SMOW}$ ranging from +12.42 to +14.81 ‰ (Table 3). Similar values were obtained by Schönenberger & Markl (2008) for acid rinsed whole-rock samples from the FDC and from late-stage vein calcite from the FDC. The MSC samples span a larger range than the FDC with generally higher $\delta^{13}C_{PDB}$ from -1 to -3 ‰ and higher $\delta^{18}O_{SMOW}$ values of +12 to +20 ‰. There is no relationship between degree of alteration in hand specimen with the C and O isotope ratios.

Data from the MSC, FDC and carbonatite in the diatreme are plotted as $\delta^{18}O$ versus $\delta^{13}C$ (Fig. 5). Additional data from the FDC (Schönenberger & Markl 2008), the fields for Igaliko and Grønnedal-Íka carbonatite (Coulson *et al.*, 2003; Goodenough, 1997; Pearce & Leng, 1996 and Pearce *et al.*, 1997) and O and C isotope compositions of mantle-derived carbonatite (Keller & Hoefs, 1995; Taylor *et al.*, 1967) are added for reference. Samples from the FDC and MSC plot within two discrete groups, each showing considerable range in both isotopes with several samples show high (>20 ‰) $\delta^{18}O$ values. This is most apparent in the MSC – Altered Nepheline Syenites which shows a notably larger range for both $\delta^{13}C$ and $\delta^{18}O$ than the FDC. Samples from the MSC have $\delta^{13}C$ values which are between 0.3-2 ‰ higher than the FDC.

Lu-Hf Isotopic Data

Lu and Hf isotopic data were collected from the zircon of zircon-astrophyllite pegmatite facies of MSC - Altered Nepheline Syenite at Locations 4 and 1 (Fig. 1, Supplementary data). For melting of a simple mantle source, the resultant magma would have Lu-Hf ages that lie to the depleted mantle evolution line at the crystallization age of the zircon (Fig. 6). Subsequent radiogenic decay of ^{176}Lu increases the $^{176}Hf/^{177}Hf$ ratio, and this is corrected to provide an initial $^{176}Hf/^{177}Hf$ estimate at the time of zircon crystallisation. Data are corrected for Lu decay using independent U-Pb age estimates for each point (McCreath *et al.* 2012, Table 1). Fig. 6 presents the age corrected Hf

isotopic ratio together with evolution lines for depleted mantle and CHUR. Two datasets from different parts of the Motzfeldt Sø Centre overlap within error and are here considered together.

The zircon of the MSC – Altered Nepheline Syenite was shown by McCreath *et al.* (2012) to have been substantially altered by late-stage hydrothermal activity, imaged by cathodoluminescence. We have therefore first examined the Lu-Hf data as a function of the alteration (light and dark blue points on McCreath *et al.* 2012, Fig. 5). There is no significant difference between data in 'fresh' and 'altered' regions, in contrast to U-Pb data (McCreath *et al.* 2012) where altered regions are predominantly discordant. A two-tailed student's 't' test assuming equal variance on the means of altered and unaltered initial $^{176}Hf/^{177}Hf$ ratios shows no significant difference (P=0.36 and is >> 0.05). We therefore infer that the alteration has not disrupted the Lu-Hf systematics and disregard alteration in our subsequent analysis below.

DISCUSSION AND GENESIS MODEL

Magma Sources

The magmas of the Gardar Province are inferred to have been derived from adiabatic melting of a mantle source (e.g. Upton *et al.* 2003). The primitive magmas are considered to be alkaline olivine basalt, which fractionated through intermediate rocks to provide the evolved compositions that now constitute the Gardar central complexes. However the Lu-Hf data lie significantly below the composition of mantle in Early Gardar times (Fig. 6). Projecting the data back to the Depleted Mantle line using a range of Lu/Hf ratios (0.000-0.034) is consistent with a single mantle source with a separation age ~1.86 Ga, i.e., broadly the age of the Ketilidian basement into which Motzfeldt is intruded. One might infer that all the Hf at Motzfeldt is derived from Ketilidian basement. However that would indicate that primary Early Gardar magmas contained negligible Hf, inconsistent with our understanding of the evolution of Gardar magmas (Upton *et al.* 2003). Furthermore such a very large range of Lu/Hf ratios (0.000-0.034) is unlikely. Alternatively, a similar spread of Hf data could be achieved by mixing different proportions of older, i.e. Palaeoproterozoic or Archaean, Hf (whose evolution lines follow the grey slopes, Fig. 6) with juvenile, Early Gardar Hf whose composition lies on the green point. The data indicate that Hf at Motzfeldt included contemporary mantle Hf mixed with a significant component of a pre-Gardar source. Similar models, invoking mixing of old Hf components with contemporary Hf have been proposed in other locations (e.g. Andersen 2007, Heinonen *et al.* 2010). Mixing of contemporary Early Gardar with Palaeoproterozoic or Archaean sources are consistent with the Hf signatures observed. Archaean rocks are not exposed at the surface but the presence of Archaean rocks at

depth has been suggested (e.g. Steenfelt *et al.* 2016). Andersen (2013) showed that some zircons in the Eriksfjord Formation were of Archaean (2.5 Ga and older) ages. A full interpretation of the regional significance of these Hf isotopic data is beyond the present study but the data provide evidence that Motzfeldt Hf had multiple sources. We infer that these include a component from melting of Early Gardar asthenospheric mantle, plus an older, possible Archaean, Hf-rich component. We cannot rule out smaller contributions of Ketilidian Hf from local crustal contamination.

Although Hf is an important critical metal, the primary target for exploration at Motzfeldt has been Nb and Ta. Ideally one would use isotopes of those metals to explore the genesis of these and other HFSE. However, Nb only has one isotope and, as yet, an understanding of the geological histories encoded in the isotopes of Ta is undeveloped. HFSE act together in the melting and assimilation processes (e.g. Pearce & Peate 1995). We therefore extend the inferences drawn from Hf data to other HFSE and suggest that Nb and Ta at Motzfeldt also had multiple sources. One might speculate whether Motzfeldt Nb and Ta enrichment owes its existence to the fact that HFSE have multiple sources.

Fractionation, Ascent, Emplacement and Final Structure

Evolved rocks across the Gardar Province formed by fractional crystallisation producing coherent geochemical trends from basic to intermediate to evolved rocks (e.g. Upton & Emeleus 1987, Upton *et al.* 2003). Although few basic to intermediate rocks are preserved at Motzfeldt, we infer similarly that the Motzfeldt magmas were the products of fractionation in the crust of mantle-derived melts. Syenite and nepheline syenite magmas are buoyant and rise through the crust. In the context of Motzfeldt, we infer that these magmas exploited pre-existing fault systems reactivated by the Early Gardar rifting. The region was active over a prolonged period (Table 1) forming a long-lived volcanic system and from field relationships, we conclude that current exposure is very close to the roof zone. By analogy with East Africa (e,g, the Kone volcanic centre, Rampey *et al.* 2010), we conclude that each centre lay beneath and fed a volcano on the Gardar land surface. The unconformity between the Ketilidian basement and the overlying Eriksfjord formation is preserved immediately to the North of Motzfeldt (Fig. 1). We do not consider it coincidence that this unconformity is preserved so close to the roof and we consider the unconformity to have formed a horizontal decollement within the crust that impeded ascent of the syenite magma and against which Motzfeldt Sø Centre magmas ponded (cf. Upton 2013). The attitude of vertical slices through the contacts support the view that emplacement of the magma was achieved by caldera collapse, stoping coupled with transtensional fault movements. We also observe that the magma intruded the

roof and sides of the chamber by sheeting into the country rocks, progressively detaching and decoupling large rafts from the roof and sides which then sank within the chamber. The paucity of arenite xenoliths within the syenite, compared to those *in situ*, hints that these were rapidly digested in the magma. Either because of density stratification, or because of localised crustal contamination by silica-rich Eriksfjord arenites at the roof, the roof zone is silica oversaturated whereas the lower parts of the chamber are nepheline bearing. Although carbonate and fluorite are common hydrothermal minerals in the Motzfeldt Sø Centre, we find little evidence for carbonate or fluoride melts in this system (cf. Vasyukova & Williams-Jones 2014).

Synthesis of Overall Structure

Fig. 1 summarises all published field data integrated with our own field studies. The E-W movement on the Flinks Dal Fault can be estimated by the offset to the eastern boundary of the complex. From this, 6 km of sinistral movement along this and other minor faults is inferred. To explore the original disposition of the volcanic centres, we reconstruct the geology of the area by reversing the fault displacements and extrapolating the geology across the fjords (Fig. 7). Such a reconstruction allows the original geometry of the complex to be appreciated. The reconstruction places MSC rocks south of Flinks Dal directly opposite rocks of the North Qôroq Centre and the match of these two units across the fault is striking. From this, we hypothesise that rocks interpreted by Tukiainen (1988) as MSC are rather an extension of North Qôroq Centre, and this resolves the internal inconsistency in the relative age of the MSC in the Tukiainen (1988) map (MSC appears younger than FDC in the south but older in the north). This reconstruction shows the North Qôroq – Motzfeldt region as a series of overlapping, elliptical subvolcanic centres broadly aligned with their long axes E-W, the direction perpendicular to regional extension in Early Gardar times (Bartels *et al.* 2015). The Motzfeldt Sø Centre, the earliest phase of activity, is dated at 1273 ± 6 and 1275 ± 1 Ma (McCreath *et al.* 2012, Salmon 2013 respectively, Table 1) and possibly the youngest, North Motzfeldt, is dated as 1257 ± 7 Ma (Salmon 2013). These precise U-Pb data indicate that the Motzfeldt region was volcanically active for 15-20 Ma. This reconstruction fits in terms of size and duration with modern volcanic constructs in East Africa (e.g., the Kone volcanic system, Rampey *et al.* 2010) where the locus of magmatism evolves with time over 10s km to create a volcanic range whose morphology is dictated by regional structural control (e.g. Acocella *et al.* 2002, Wiart & Oppenheimer 2005).

The magmas of the Motzfeldt Sø Centre ponded and chilled against the roof and current exposure now preserves the complex interactions between magma and roof (Fig. 8). Interaction between nepheline syenite magma and arenites in the roof zone led to strong gradients in silica

activity and possibly other elements such as fluorine. The roof zone comprised an isolated lens of magma which had a lower density, was more silica rich and more evolved than the remainder of the complex. Magma sheeted into the roof zone and chilled against it, providing a zone comprising partially crystallised, hot magmas which were then repeated sheeted from below by other syenite variants. This is now expressed as a region of cross-cutting inclined sheets of fine- to coarse-grained syenite variants which lack chilled margins. We call this zone the 'Hot Sheeted Roof'. Some of these variants were rich in HFSE and crystallised pyrochlore. It may be that these exceptionally pyrochlore-rich rocks formed as crystal sediments in lower parts of the roof zone, separating physically from less dense minerals such as feldspar and feldspathoids. Perhaps through overturn, or episodic events such as faulting or replenishment, the pyrochlore-rich variants were drawn into higher levels of the roof, adding networks of pyrochlore microsyenite units to the 'Hot Sheeted Roof'. These now form the series of discontinuous inclined sheets without chilled margins that are observed.

The NE-SW giant alkali gabbro dyke at Motzfeldt cuts all rocks in the region and its orientation is parallel to smaller Late Gardar dykes. Its orientation represents Late Gardar, rather than Early Gardar, extension. We interpret this giant dyke as a late Gardar feature related to the Tugtutôq-Ilímaussaq-Nunataq dyke swarm ~100 Ma later than the events at the Motzfeldt Sø Centre.

Hydrothermal Alteration

Hand specimens show evidence for pervasive alteration for many parts in the Motzfeldt Sø Centre, expressed by i) hematite staining and turbidity in alkali feldspar, ii) alteration of pyroxene and amphibole to knots of Fe-rich oxides and hydroxides, iii) formation of secondary biotite mica as overgrowths on ilmenomagnetite, iv) precipitation of carbonates, fluorite and minor REE-rich phases along cleavage planes in feldspar, v) transport of U, Na and other elements in the late-stage fluids expressed in the compositions of secondary zircon (McCreath *et al.* 2013), vi) opening of the U-Pb isotopic system in zircon (McCreath *et al.* 2012). Most, but not all, of the Motzfeldt Sø Centre is altered by this fluid.

The multiple expressions of alteration at Motzfeldt are unlikely to be the product of a single fluid phase at a single temperature. In the simplest scenario, these types of alteration may represent the action of a single juvenile fluid as it cooled from post-magmatic temperatures. However more complex models, involving multiple fluids of different sources (meteoric vs magmatic), salinities, pHs, redox state and temperatures may also be relevant. Whereas detailed fluid inclusion studies allow fluid evolution to be reconstructed in many mineral deposits (e.g. Salvi & Williams-Jones 1990), fluid inclusions in alkali feldspar at Motzfeldt have leaked substantially and provide

inconsistent and unsatisfactory results (McCreath 2009). Therefore the chemical and isotopic nature of the fluid must be determined indirectly from other indicators.

The fluorine contents of biotite provide insights into the F-content of late-stage fluids (e.g. Munoz 1984). This method was used by Finch (1995) and Finch *et al.* (1995) to understand how the F contents of late-stage fluids changes across the Gardar Province. Briefly, these studies showed that F vs atomic Fe/(Fe+Mg) within biotite plotted as right-angled triangular fields, the slopes of which change from centre to centre across the Gardar Province. The slope of this 'Maximum Fluorine' line reflects the relative F content of the late-stage fluids associated with each centre, assuming that the temperature of the interaction is the same. It is inferred that the steeper slopes have higher F contents (Finch 1995, Finch *et al.* 1995), although the authors showed that uncertainties in temperature and the partitioning of F between fluid and biotite meant that they were unable to calculate meaningful F activities. Finch *et al.* (1995) were, however, able to demonstrate significant relative variations between different Gardar subvolcanic centres in the F contents of the fluid at biotite closure.

Finch *et al.* (1995) showed that the Motzfeldt centre has one of the highest fluorine activities within the province, comparable to the Late Igdlerfigssalik and altered South Qôroq units (Finch 1995). They found no systematic differences in the halogen content of biotite in individual units of the Motzfeldt region, but their analyses were restricted to the FDC and avoided the pervasive alteration in the North and North-East. There are suggestions that the halogen content and fluid evolution of the Motzfeldt Sø Centre played an important role in the genesis of the mineralisation within this centre (Bradshaw, 1988; Jones, 1980). As part of the present study, we collect biotite data from the Motzfeldt Sø and Flinks Dal Centres. Comparison of the present data with those of Finch *et al.* (1995) (Fig. 4) confirms that the Maximum Fluorine Line from the FDC and Finch *et al.* (1995) coincide. However, comparison of the data for the MSC and FDC shows that MSC biotite has more F for the same Fe/(Fe+Mg) and the Maximum Fluorine Line is steeper (Fig. 4). From this we infer that fluids associated with the MSC are more F-rich than those of the FDC. Similarly higher F contents are found for biotite collected from syenite taken immediately underneath Eriksfjord rafts within the FDC (Fig. 4) which suggests that the environments under the rafts are similarly volatile rich in a manner akin to the roof zone.

The hydrothermal fluid also altered the pyrochlore, importing elements such as U, Th and Pb (McCreath *et al.* 2013) and opening the U-Pb isotopic system (McCreath *et al.* 2012). McCreath *et al.* (2012) showed that hydrothermal episode followed magmatism within error of the age estimates i.e. <6 Ma (to 95% confidence). Our EPMA maps are consistent with McCreath *et al.*'s hypothesis that the alteration mobilised 'A'-site elements in the pyrochlore (including Na, Ca, U) but did not

transport those on the 'B'-site (Nb and Ta), which retain magmatic oscillatory zoning (Fig. 3). Although mobility in some HFSE in this environment is feasible, the Nb and Ta content of the pyrochlore remained essentially constant during alteration (McCreath *et al.* 2013, Fig. 3), and hydrothermal alteration did not influence Hf isotope data in zircon (Fig. 6). We contrast this fluorine-rich hydrothermal environment, in which HFSE were immobile, with that of Timofeev & Williams-Jones (2015) where the converse was true. Mobility of HFSE may not be a simple function of F content in the fluid, but rather a combination of F and other parameters such as pH and redox state. Nevertheless, it is inferred that the exceptional F content of the fluid is implicated in the subsolidus mobility of many other elements at Motzfeldt such as U, Th and Pb. The product of this mobility and alteration includes the intimate (nm-scale) intergrowths of different pyrochlore supergroup minerals (see McCreath *et al.* 2013, Fig. 3). A radiometric airborne survey was carried out by Angus and Ross plc over some of the licence area. Within Motzfeldt, U contents vary by orders of magnitude even within the same geological unit. This is because mapping defines suites of syenite variants, rather than individual lithologies, and U is heterogeneously distributed across the many variants. Analysis of the MSC rocks showed U to be hosted in pyrochlore and hence, in the initial stages of exploration, the radiometric map was used to direct exploration for pyrochlore. However detailed mineralogical analysis showed that addition of further U into the pyrochlore was secondary (McCreath *et al.* 2012, 2013), hence the maxima in the radiometric map delimit the extent of *hydrothermally altered* pyrochlore and not the primary pyrochlore itself.

Carbon and oxygen stable isotopes in carbonate have been studied to determine the provenance and evolution of these elements in the Motzfeldt rocks (Fig. 5). The data of the present study are similar to results for other Igaliko carbonate (Pearce & Leng 1996; Coulson *et al.* 2003). Mantle-derived carbonate has $\delta^{18}O$ and $\delta^{13}C$ between +6 and +10 ‰ and -8 and -4 ‰, respectively (Keller & Hoefs, 1995; Taylor *et al.* 1967, Fig. 5). Carbonatite and lamprophyre units in the Igaliko Complex are considered to be of primitive mantle origin, though they deviate from exclusively mantle isotopic signatures. $\delta^{13}C$ for the FDC generally falls within the -8 to -4 ‰ range of mantle carbon, however the $\delta^{13}C$ from the MSC is slightly richer in ^{13}C than mantle. C and O isotope variation in carbonatite is commonly reported in shallow level intrusions (e.g. Andersen 1987; Nielsen & Buchart 1985; Reid & Cooper 1992), but determining the processes which generate such changes is problematic (Fig. 5). Such variations have in the past been interpreted as a combination of fractionation, crustal assimilation and subsolidus re-equilibration (e.g. Coulson *et al.* 2003).

The stable isotope data are consistent with carbonate in the MSC and FDC as dominantly of mantle origin, but modified either during magma evolution or in the subsolidus. The influence that a variety of potential geological processes would have on oxygen and carbon isotope data values is

shown as vectors on Fig. 5b. The data rule out the influx of meteoric waters ($\delta^{13}C$ and $\delta^{18}O \approx 0$; Javoy *et al.* 1986, Kah & Bartley 2011) drawing O and C isotope values towards the origin (Fig. 5). Rather, the data show $\delta^{18}O$ higher than mantle values. With continued Rayleigh fractionation progressively more evolved melts fractions became depleted with respect to light carbon and oxygen as mantle CO_2 is partitioned between crystallising carbonate and coexisting vapour. This process would produce an increase in $\delta^{18}O$ and, to a lesser degree, $\delta^{13}C$ as fractionation progressed (Deines, 1970; 1989; Nielsen & Buchart, 1985; Pearce & Leng, 1996). This model was proposed by Pearce & Leng (1996) for the evolution of the Igaliko dyke swarm and by Tichomirowa *et al.* (2006) for the Tiksheozero and Siilinjarvi carbonatites of the Kola province. Alternatively, one might envisage this process occurring not in the magma, but as carbothermal residua re-equilibrate with their host rocks at low temperatures in the subsolidus (Deines 1989; Demény *et al.* 1998; Sharp 2007). Coulson *et al.* (2003) called upon fractionation, possibly enhanced by isotopic shifts associated with the formation of fluorcarbonate ions, to explain a similar range of data at North Qôroq.

Isotopic compositions can also be modified by assimilation of rocks enriched in ^{13}C and ^{18}O. Ketilidian rocks have C and O isotope signatures that broadly match a mantle source, hence assimilation of local basement would not influence ^{13}C and ^{18}O. However at Motzfeldt, there is field evidence to demonstrate assimilation of Eriksfjord sedimentary rocks (Bradshaw 1998, Jones 1980, Fig. 2). The field of sedimentary carbonate is shown in Fig. 5 and lies along a similar vector to that inferred from fractionation. Therefore at Motzfeldt, one cannot differentiate with certainty between the influence of fractionation and assimilation of local Eriksfjord. The greater spread of data in the MSC (which cuts Eriksfjord rocks) compared to the FDC (which only cuts other syenites) hints that both fractionation and assimilation are at work in the MSC whereas fractionation alone modified the compositions of the FDC.

The widespread formation of hematite in the MSC provides the characteristic red colour of the region and indicates that during the sub-solidus fO_2 of the fluid increased above the hematite-magnetite buffer. This predated emplacement of the MSC – Peralkaline Sheets, Flinks Dal Centre (McCreath 2009) and North Motzfeldt Centre (Finch *et al.* 2001, Salmon 2013), which retain fresh unaltered feldspar. The hematite is often localised around mafic minerals, consistent with the suggestion that it is formed from the breakdown of arfvedsonite and aegirine. Bradshaw (1988) and Schönenberger & Markl (2008) invoked the collapse of a magmatic hydrothermal system on cooling and a subsequent influx of oxidised groundwater to account for the presence of hematite and a similar model was suggested by Köhler *et al.* (2008) for the fluid evolution of the Ivigtût

complex. However the carbon and oxygen isotopes of carbonate at Motzfeldt do not indicate meteoric input (cf. Vasyukova & Williams-Jones 2017).

Exploration Implications of the Model

The genetic model rationalises the complex geology at Motzfeldt and provides several pointers for exploration. First, the unusually high modal pyrochlore is a consequence of the exceptional HFSE content in the magma, which was derived from multiple HFSE sources. Enhanced HFSE contents at source were amplified through fractionation and one might speculate that it was because of the multiple components to the HFSE budget at source, that this magma formed rocks of commercial interest. The magma ascended, was emplaced at the unconformity of sediments and basement by the 'Hot Sheeted Roof' model, whereby magma variants repeated sheet into the roof, quickly becoming plastic and avoiding chilled contacts. The rocks formed are definable suites of syenite variants, not single rocks with fixed mineralogy and texture. Second, the Nb and Ta contents of the pyrochlore are magmatic features. The very friable, altered nature of the Motzfeldt Sø Centre syenite is in stark contrast with very fresh rocks that characterise the majority of the Gardar. The fluid was exceptionally F-rich, and one of the most fluorine-rich environments throughout the province. However, the alteration had no effect on the concentration of Ta and Nb, although it transported substantial volumes of other elements, including U and Pb (McCreath *et al.* 2012, 2013). It should be noted that in the early stages of the Motzfeldt project, the coincidence of pyrochlore finds and the striking colour of the alteration led to the assumption that the grade was enhanced by the hydrothermal activity. This is not the case. Third, the targets in the early stages of exploration were chosen following radiometric survey. Radiometric maxima delimit ***remobilisation of U during hydrothermal alteration***, rather than the distribution of primary pyrochlore. The very intimate U-rich intergrowths in hydrothermally altered pyrochlore (see McCreath et al. 2013) make for slow and difficult dissolution and the tailings from the site would be potentially radioactive. The optimum target is pyrochlore that has avoided hydrothermal alteration, i.e. pyrochlore-rich microsyenite outside the radiometric hot-spots.

CONCLUSIONS

The present paper provides the first genetic model for a syenite-hosted Nb-Ta deposit. We bring together evidence for the evolution of the deposit from magma genesis to crystallisation and hydrothermal alteration. Using Hf isotopes, we show that the magma contained an older, Archaean Hf component, mixed with contemporary asthenospheric Hf, and we infer that all the high field

strength elements similarly had mixed sources. Fractionation occurred during ascent and a series of evolved nepheline syenite magmas were emplaced at shallow (~3 km depth) levels in the crust at the unconformity between basement Ketilidian rocks and the overlying Eriksfjord supracrustals. Substantial (>3 km diameter) magma chambers were formed, feeding volcanic constructs on the Gardar land surface. Fluorine content of biotite is used to indicate that exceptional fluorine concentrations were developed under large (~1 km diameter) xenoliths and in the roof zone. Perhaps assisted by the high fluorine levels, assimilation of Eriksfjord arenite in the roof zone took place, locally pushing the syenite melt composition into the quartz syenite field, even though nepheline syenite magma remained at depth. As the magma in the roof cooled, it started to solidify and became plastic. Repeated sheeting of multiple syenite variants into the roof zone, including pyrochlore-rich microsyenite, took place providing a heterogeneous syenite suite rather than a single lithology (the 'Hot Sheeted Roof' model). After crystallisation of the melt, fluorine-rich hydrothermal fluids altered the pyrochlore, feldspars and mafic minerals, creating the strikingly red hematite-rich alkali feldspar that characterises the area. The fluid mobilised many elements, including U, Pb and Th, which chemically and isotopically modified many minerals including zircon and pyrochlore. However, despite the exceptional F activity, most HFSE were immobile and Hf isotope compositions were unaffected. The Ta and Nb contents of the pyrochlore were unchanged, but U and Pb were introduced. The resulting altered pyrochlore is an intimate (nm-scale) intergrowth of many generations of pyrochlore group minerals that pose challenges for efficient extraction. Once the area was identified as a potential Nb and Ta deposit, U and Th radiometric survey was used to identify targets and as the basis for resource estimation. However U and Th signals identify *altered* pyrochlore, which provides the most challenging metallurgy and the poorest yields. This approach potentially underestimates the size of the resource and processing of such material would maximise U and Th in tailings. We show that Ta is also present in less altered pyrochlore in other, less uraniferous, parts of the Motzfeldt Sø Centre and its compositional state is less complex. Some of these are of a lower overall grade, but may yield more efficient extraction and fewer radioactive tailings. Radiometric survey of such a deposit may require careful consideration before identification of key targets.

Repeated magmatism on similar foci took place after the formation of the Motzfeldt Sø Centre (the area of commercial interest) creating a complex of overlapping syenite centres. A reappraisal of the geology of Motzfeldt – North Qôroq area is presented, including a reconstruction of the geology prior to the lateral displacement on faults. Dating of the North Motzfeldt centre, one of the youngest in the area, indicates that the system was active for ~ 15-20 Ma. The Motzfeldt area compares favourably to modern volcanic systems in the East African Rift, both in terms of its size and the period of activity.

REFERENCES

Acocella V, Korme T, Salvini F & Funicello R (2002) Elliptic Calderas in the Ethiopian Rift: Control of Pre-Existing Structures. *Journal of Volcanology and Geothermal Research*, **119**, 189-203.

Allaart JH (1967) Basic and Intermediate Igneous Activity and its Relationships to the Evolution of the Julianehåb Granite, South Greenland. *Meddelelser om Grønland*, **175**, No. 1, 136pp.

Andersen T (1987) Mantle and crustal components in a carbonatite complex, and the evolution of carbonatite magma: REE and isotopic evidence from the Fen complex, SE Norway. *Chemical Geology (Isotope Geoscience Section)* **65**, 147-166

Andersen T (2007) Sveconorwegian crustal underplating in southwestern Fennoscandia:LAM-ICPMS U–Pb and Lu–Hf isotope evidence from granites and gneisses in Telemark, S Norway. *Lithos* **93**, 273–287

Andersen T (2013) Age, Hf isotope and trace element signatures of detrital zircons in the Mesoproterozoic Eriksfjord sandstone, southern Greenland: are detrital zircons reliable guides to sedimentary provenance and timing of deposition? *Geological Magazine* **150**, 426-440.

Armour-Brown A, Tukiainen T, Wallin B, Bradshaw C & Emeleus CH (1983) Uranium exploration in South Greenland. *Rapport Grønlands Geologiske Undersøgelse* **115**, 68-75.

Bailey SW (1984) Classification and structures of the micas. In: SW Bailey (Ed.) *Micas: Reviews in Mineralogy and Geochemistry, Mineralogical Society of America* **13**, 1-12.

Bartels A, Nielsen TFD, Lee SR & Upton BGJ (2015) Petrological and geochemical characteristics of Mesoproterozoic dyke swarms in the Gardar Province, South Greenland: Evidence for a major sub-continental lithospheric mantle component in the generation of the magmas. *Mineralogical Magazine* **79**, 909-939.

Blaxland AB, van Breemen O, Emeleus CH & Anderson JG (1978) Age and origin of major syenite centers in Gardar Province of South Greenland - Rb-Sr studies. *Geological Society of America Bulletin* **89**, 231-244.

Bradshaw C (1985) The Alkaline rocks of the Motzfeldt Centre: Progress report on the 1984 field season. *Rapport Grønlands Geologiske Undersøgelse* **125**, 62-64.

Bradshaw C (1988) A petrographic, structural and geochemical study of the alkaline igneous rocks of the Motzfeldt centre, South Greenland. *Unpublished PhD thesis*, University of Durham, UK.

British Geological Survey (2012) *Risk List 2012: An update to the supply risk index for elements or element groups that are of economic value*. British Geological Survey, UK, 12pp.

Chadwick B & Garde AA (1996) Palaeoproterozoic oblique plate convergence in South Greenland: a reappraisal of the Ketilidian Orogen. *Geological Society, London, Special Publications* **112**, 179-196.

Chambers AD (1976) *The Petrology and Geochemistry of the North Qôroq Centre, Igaliko Complex, S Greenland*. Unpubl. PhD thesis, University of Durham, UK.

Coulson IM (1996) Rare-earth and High-Field-Strength Element Mobility in and around the North Qôroq centre, Gardar province of South Greenland. Unpubl. PhD thesis, University of Birmingham, UK.

Coulson IM, Goodenough KM, Pearce NJG and Leng MJ (2003) Carbonatites and lamprophyres of the Gardar province – a window to the sub-Gardar Mantle? *Mineralogical Magazine* **67**, 855-872.

Deines P (1970) Carbon and oxygen isotopic composition of carbonates from the Oka carbonatite, Quebec, Canada. *Geochimica et Cosmochimica Acta* **34**, 1199-1225.

Deines P (1989) Stable isotope variations in carbonatites. In: K Bell (Ed.) *Carbonatites: Genesis and Evolution*, 301-59. Unwin and Hyman, London.

Demény A, Ahijado A, Casillas R & Vennemann T (1998) Crustal contamination and fluid/rock interaction in the carbonatites of Fuerteventura (Canary Islands, Spain): A C, O, H isotope study. *Lithos* **44**, 101-15.

Elburg MA, Andersen T, Bons PD, Simonsen SL & Weisheit A (2013) New constraints on Phanerozoic magmatic and hydrothermal events in the Mt Painter Province, South Australia. *Gondwana Research*, **24**, 700-712.

Emeleus CH & Harry WT (1970) The Igaliko Nepheline Syenite Complex, South Greenland. *Meddelelser om Grønland*, **186**, no. 3, 116pp.

European Commission (2014) Report on Critical Raw Materials for the EU, Report of the Ad hoc Working Group on defining critical raw materials. Accessed Dec 2016: http://ec.europa.eu/DocsRoom/documents/10010/attachments/1/translations

Finch AA (1995) Metasomatic overprinting by juvenile igneous fluids, Igdlerfigsalik, S Greenland. *Contributions to Mineralogy & Petrology* **122**, 11-24.

Finch AA, Parsons I & Mingard SC (1995) Biotites as indicators of fluorine fugacities in fluids associated with alkaline magmatism: the Gardar province of S Greenland. *Journal of Petrology* **36**, 1701-1728.

Finch AA, Goodenough KM, Salmon HM & Andersen T (2001) The Petrology and Petrogenesis of the North Motzfeldt Syenites. *Mineralogical Magazine*, **65**, 797-812.

Goodenough KM (1997) Geochemistry of Gardar intrusions in the Ivigtût area, South Greenland. Unpub. PhD thesis. University of Edinburgh, UK.

Heinonen AP, Andersen T & Rämö OT (2010) Re-evaluation of Rapakivi Petrogenesis: Source Constraints from the Hf Isotope Composition of Zircon in the Rapakivi Granites and associated Mafic Rocks of Southern Finland. *Journal of Petrology*, **51**, 1687-1709.

Jones AP (1980) The petrology and structure of the Motzfeldt centre, Igaliko, South Greenland. *Unpublished PhD thesis*. University of Durham, UK.

Javoy M, Pineay F & Delorme H (1986) Carbon and nitrogen isotopes in the mantle. *Chemical Geology* **57**, 41-62.

Kah LC & Bartley JK (2011) Protracted oxygenation of the Proterozoic biosphere. *International Geology Review*, **53**, 1424-1442.

Keller J & Hoefs J (1995) Stable isotope characteristics of recent natrocarbonatites from Oldoinya Lengai. In K Bell & J Keller (Eds) *Carbonatite volcanism: Oldoinya Lengai and the petrogenesis of natrocarbonatites*. IAVCEI proceedings in volcanology 4. Springer, Berlin.

Köhler J, Konnerup-Madsen J & Markl G (2008) Fluid chemistry in the Ivigtût cryolite deposit, South Greenland. *Lithos* **103**, 369-92.

Le Maitre RW (ed.) (2002) *Igneous Rocks: A Classification and Glossary of Terms*. Cambridge University Press, 236pp.

Mackay DAR & Simandl GJ (2014) Geology, market and supply chain of niobium and tantalum—a review. *Mineralium deposita* **49**, 1025-1047.

McCreath, JA (2009) Petrology and petrogenesis of the Motzfeldt Ta-mineralisation, Gardar Province, South Greenland. *Unpublished PhD thesis*, University of St Andrews, UK.

McCreath JA, Finch AA, Simonsen SL, Donaldson CH & Armour-Brown A (2012) Independent ages of magmatic and hydrothermal activity in alkaline igneous rocks: The Motzfeldt Centre, Gardar Province, South Greenland. *Contributions to Mineralogy and Petrology* **163**, 967-982.

McCreath JA, Finch AA, Herd DA & Armour-Brown A (2013) Geochemistry of Pyrochlore Mineralogy from the Motzfeldt Centre, South Greenland: The Mineralogy of a Syenite-hosted Ta, Nb Deposit. *American Mineralogist* **98**, 426-438.

Melcher et al. (2008) Fingerprinting of conflict minerals: columbite-tantalite ('coltan') ores. *SGA News*, **23**, 1-14.

Melcher et al. (2015) Tantalum–(niobium–tin) mineralisation in African pegmatites and rare metal granites: Constraints from Ta–Nb oxide mineralogy, geochemistry and U–Pb geochronology. *Ore Geology Reviews*, **64**, 667-719.

Munoz J (1984) F-OH and Cl-OH exchange in micas with applications to hydrothermal ore deposits. In S.W. Bailey, Ed., *Micas: Reviews in Mineralogy and Geochemistry, Mineralogical Society of America*, **13**, 469-94.

Nielsen TFD & Buchardt B (1985) Sr-C-O isotopes in nephelinitic rocks and carbonatites, Gardiner Complex, Tertiary of East Greenland. *Chemical Geology* **53**, 207-17

Parsons I, Mason RA, Becker SM & Finch AA (1991) Biotite equilibria and fluid circulation in the Klokken intrusion. *Journal of Petrology* **32**, 1299-1333.

Paslick CR, Halliday AN, Davies GR, Mezger K & Upton BGJ (1993): Timing of Proterozoic magmatism in the Gardar Province, southern Greenland. *Geological Society of America Bulletin*, **105**, 272-278.

Patchett, PJ & Tatsumoto M (1980) A routine high-precision method for Lu-Hf isotope geochemistry and chronology. *Contributions to Mineralogy and Petrology*, **75**, 263-267.

Pearce JA & Peate DW (1995) Tectonic implications of the compositions of volcanic arc magmas. *Annual Review of Earth and Planetary Sciences*, **23**, 251-285.

Pearce NJG & Leng M (1996) The origin of carbonatites and related rocks from the Igaliko dyke swarm, Gardar Province, South Greenland: Field geochemical and C-O-Sr-Nd isotope evidence. *Lithos* **39**, 21-40.

Pearce NJG, Leng M, Emeleus CH & Bedford C (1997) The origins of carbonatites and related rocks from the Grønnedal-Ika nepheline syenite complex, South Greenland: C-O-Sr isotope evidence. *Mineralogical Magazine* **61**, 515-29.

Poulsen V (1964) The sandstones of the Precambrian Eriksfjord Formation in South Greenland. *Rapport Grønlands Geologiske Undersøgelse* **2**, 16.

Rampey ML, Oppenheimer C, Pyle DM & Yirgu G (2010) Caldera-forming eruptions of the Quaternary Kone Volcanic Complex, Ethiopia. *Journal of African Earth Sciences* **58**, 51-66.

Reid D & Cooper A (1992) Oxygen and carbon isotope patterns in the Dicker Willem carbonatite complex, southern Namibia. *Chemical Geology* **94**, 293-305.

Salmon HM (2013) The Mineralogy and Petrology of Satellitic Intrusions within the Igaliku Complex, South Greenland. Unpubl. PhD Thesis, Birkbeck College, University of London, UK.

Salvi S & Williams-Jones AE (1990) The role of hydrothermal processes in the granite-hosted Zy, Y, REE deposit at Strange Lake, Québec-Labrador: Evidence from fluid inclusions. *Geochimica et Cosmochimica Acta* **54**, 2403-2418.

Schönenberger J & Markl G (2008) The magmatic and fluid evolution of the Motzfeldt intrusion in South Greenland: Insights into the formation of agpaitic and miaskitic rocks. *Journal of Petrology* **49**, 1549-1577.

Sharp Z (2007) *Principles of Stable Isotope Geology*. Prentice Hall, New Jersey, USA.

Steenfeld A, Kolb J & Thrane K (2016) Metallogeny of South Greenland: A review of geological evolution, mineral occurrences and geochemical exploration data. *Ore Geology Reviews* **77**, 194-245.

Taylor H, Frechen J & Degens E (1967) Oxygen and carbon isotope studies of carbonatites from the Laacher See district, West Germany and the Alnö District Sweden. *Geochimica et Cosmochimica Acta* **31**, 407-30.

Tichomirowa M, Grosch G, Gotze J, Baltyatsky BV, Savva EV, Keller J & Todt W (2006) The mineral isotopic composition of two Precambrian carbonatite complexes from the Kola alkaline Province – Alteration versus primary magmatic signatures. *Lithos* **91**, 229-49.

Timofeev A & Williams-Jones AE (2015) The Origin of Niobium and Tantalum Mineralisation in the Nechalacho REE Deposit, NWT, Canada. *Economic Geology* **110**, 1719-1735.

Tukiainen T (1988) Niobium-Tantalum Mineralisation in the Motzfeldt centre of the Igaliko Nepheline Syenite Complex, South Greenland. In: *Mineral Deposits within the European Community*, Boissonnas J and Omenetto P (eds), Springer-Verlag Berlin Heidelberg, 230-246.

Tukiainen T, Bradshaw C & Emeleus CH (1984) Geological and radiometric mapping of the Motzfeldt centre of the Igaliko Complex, South Greenland. *Rapport Grønlands Geologiske Undersøgelse* **102**, 78-83.

Upton BGJ (2013) Tectono-magmatic evolution of the younger Gardar southern rift, South Greenland. *Geological Survey of Greenland and Denmark Bulletin*, **29**, 129 pp.

Upton BGJ & Emeleus CH (1987) Mid-Proterozoic Alkaline Magmatism in Southern Greenland: The Gardar Province. In: Fitton JG & Upton BGJ (eds.) *Alkaline Igneous Rocks*, Special Publication of the Geological Society of London **30**, 449-471.

Upton BGJ, Emeleus CH, Heaman LM, Goodenough KM & Finch AA (2003) Magmatism of the Mid-Proterozoic Gardar Province, South Greenland: chronology, petrogenesis and geological setting. *Lithos*, **68**, 43-65.

US Department of Energy (2011) Critical metals strategy. US Department of Energy, 196pp

Vasyukova O & Williams-Jones AE (2014) Fluoride-silicate melt immiscibility and its role in REE ore formation: Evidence from the Strange Lake rare metal deposit, Québec-Labrador, Canada. *Geochimica et Cosmochimica Acta* **139**, 110-130.

Vasyukova O & Williams-Jones AE (2017) *Hydrothermal REE transport at Strange Lake*. Published Abstract 1467, Goldschmidt 2017, (https://goldschmidtabstracts.info/abstracts/abstractView?id=2017001467).

Wiart P & Oppenheimer C (2005) Large magnitude silicic volcanism in north Afar: the Nabro Volcanic Range and Ma'alalta volcano. *Bulletin of Volcanology* **67**, 99-115.

Zhu C & Sverjensky D (1992) F-Cl-OH partitioning between biotite and apatite. *Geochimica et Cosmochimica Acta* **56**, 3435-67.

ACKNOWLEDGEMENTS

Field visits in 2005/6 were supported by Angus and Ross plc and that in 2015 was funded by Regency Mines, the current licence holder. Dr Chris Hayward provided careful assistance on the SX-100 electron probe microanalyser at Edinburgh University. This research summarises many years of field and lab studies on the area, but the most recent work (2016) has received funding from the European Union's Horizon 2020 research and innovation programme (grant agreement No 689909). Earlier drafts of the manuscript benefitted from helpful comments from Anthony Williams-Jones and Olga Vasyukova.

APPENDIX A – PAST NOMENCLATURES FOR THE MOTZFELDT REGION

Initial mapping of Motzfeldt took place in the late 1960's in a programme sponsored by Grønlands Geologiske Undersøgelse (the Geological Survey of Greenland, GGU) published subsequent in a memoir covering the whole of the Igaliko Complex by Emeleus & Harry (1970). Those authors considered North Qôroq to be a separate centre from Motzfeldt. Within each centre, there were distinguished 5 major syenite and nepheline syenite units, prefixed SN (for North Qoroq) and SM (for Motzfeldt) and numbered 1 to 5 broadly in order of emplacement. Jones (1980) added an agpaitic syenite (SM6) and added a variant of SM4 called HY. Two main satellite syenites called the North and East Motzfeldt syenites and a syenite stock at Narsarsuaq were also identified. In the 1980s, GGU revisited the area. The area North and East of Motzfeldt Sø (Fig. 1) became the site of commercial interest when U and Ta anomalies were observed in regional sediment sampling. Detailed re-mapping of Motzfeldt commenced as part of the Syduran exploration project (Armour-Brown *et al.* 1983). Although much of this work remains outside the public domain, some has appeared in publications (Tukiainen *et al.* 1984, Tukiainen 1988, Bradshaw 1985) and a PhD thesis (Bradshaw 1988). Tukiainen *et al.* (1984) revised the field description, dividing the centre into 'Formations', a term in this context to refer to definable suites of igneous rocks. The word 'Formation', normally used to define suites of sediments, has caused difficulties for subsequent workers. To address this, we rename Tukianen's 'Formations' as 'Centres'.

Tukiainen (1988) divided the region into the Geologfjeld, Motzfeldt Sø and Flinks Dal Centres, within each of which are several subdivisions (Fig. 1, Appendix Table 1). This scheme made little reference to the nomenclature of Emeleus & Harry (1970). In detail the correlations between old and new nomenclatures are few. The SM1 and 3 units of Emeleus and Harry (1970) corresponded to the MSC and GC; SM2, 4, 5 and 6 form the FDC. SM2 and parts of SM4 together comprise the ***FDC – Porphyritic syenite***; SM5 was subdivided into the ***FDC – Nepheline syenite*** and ***FDC – Foyaite*** (meaning a nepheline syenite with a well-defined lamination, Le Maitre 2002). North Motzfeldt Centre (NMC) is considered as its own centre and no longer considered part of Geologfjeld (Finch *et al.* 2001) (Table 4). The age of the NMC can be constrained from field evidence. It is younger than the MSC since the NMC is fresh in hand specimen and avoided the pervasive regional hydrothermal alteration that characterises that centre. If the NM3 unit, which cuts NMC syenites (Finch et al. 2001), is an expression of the regional peralkaline sheeting, then the NMC is older than that sheeting episode. However the age of NMC to the Flinks Dal and North Qôroq Centres is impossible to constrain from fieldwork alone since NMC cuts neither centre. Nevertheless, radiometric age estimates of the NMC consistently place it as younger than the

majority of magmatism in the region. We therefore tentatively suggest that the NMC is one of the youngest episodes of Early Gardar magmatism in the area.

The study area comprises rocks of the GC and MSC of Bradshaw (1985, 1988). The ***GC – Nepheline Syenite*** crops out on the Northernmost corner of the centre. The MSC was subdivided into: ***MSC – Marginal Arfvedsonite Syenite***, ***MSC– Altered Nepheline Syenite*** and ***MSC – Nepheline Syenite***. Within the MSC are a number of late microsyenite sheets termed the ***MSC – Peralkaline Microsyenite Suite*** (Bradshaw 1988; Tukiainen 1988).

FIG. CAPTIONS

Fig. 1: Geological Map of the Motzfeldt-North Qôroq Volcanic System. Compilation of data from Tukiainen (1988), Bradshaw (1985), Coulson (1996), Finch *et al.* (2001) and our unpublished data. Detailed field maps of particular areas are found in supplementary information.

Fig. 2: Composite of Field Photos from the Motzfeldt Area. A – View over Location 4 (see Fig. 1) from the W. The plateau is at 1500 m and the lake in the foreground is near sea level. The view shows the table-top geography of the Motzfeldt region. B – View towards Location 5 of the Eastern edge of the Motzfeldt complex seen from Location 4. Late Gardar Basic dykes are black lines crossing the Motzfeldt syenites. The dykes appear coherent at distance, but are in reality shattered and rotated blocks sitting on top of a m-deep regolith. C – Close up of the Ta, Nb-rich syenites at Location 4. The feldspar is pink with dark arfvedsonite and metallic pyrochlore. D – Fluorite veining cutting the syenites in the roof zone at Location 4.

Fig. 3: EPMA maps of altered pyrochlore from the Motzfeldt Sø Centre. The BSE image (top left) show chaotic zoning patterns in which alteration emanates out from cracks and microfractures in the crystal. The EPMA map of Na (top right) is similarly chaotic whereas the distribution of Ta (bottom left) and Nb (bottom right) shows oscillatory zoning reminiscent of magmatic growth.

Fig. 4: Plot of atomic Fe/(Fe+Mg) versus weight percent F for samples from the Motzfeldt Sø formation, Flinks Dal Formation and sample from the underside of a basalt roof raft in

the Flinks Dal formation. The straight lines are the 'Maximum Fluorine Lines' of Finch *et al.* (1995) including their published data for the Flinks Dal Formation. The 'Mason Maximum Fluorine Line' corresponds to the maximum F possible in a biotite exhibiting complete short-range Mg-Fe order and total Fe-F avoidance. The data from the Motzfeldt Sø Formation are notably more F rich at the same Fe/(Fe+Mg) values indicating that they were in equilibrium with a more F-rich, hydrothermal fluid. Comparison of these data with Finch *et al.* (1995) indicate that the MSC was the most F-rich environment analysed within the Gardar Province.

Fig. 5: Plot of $\delta^{18}O_{SMOW}$ vs $\delta^{13}C_{PDB}$ for carbonates from the Motzfeldt Sø Formation and Flinks Dal Formation with data from carbonatite inclusions in a diatreme to the North of Motzfeldt. Top: Mantle carbonatite box from Taylor *et al.* (1967) and Keller & Hoefs (1995) shows the expected O and C isotope compositions of mantle derived carbon. Whole-rock, vein calcite and calcite crystals in fluid inclusions from the Flinks Dal formation from Schönenberger & Markl (2008) are shown (JS). Fields for Igaliko and Grønnedal-Íka carbonatites compiled from the literature are also shown. Internal precision is typically 0.01 – 0.03 ‰ for $\delta^{13}C$ and 0.01-0.03 ‰ for $\delta^{18}O$. Bottom: the mantle field is shown with vectors indicating processes that modify mantle isotope values.

Fig. 6: Lu-Hf data (corrected for Lu-decay since emplacement) from zircons from Motzfeldt versus the independent U-Pb age of the same point. Late-stage hydrothermal alteration of the zircon is evident in CL petrography (McCreath et al. 2012). Each analysis is considered either as altered (light blue) or unaltered (dark blue) – no systematic difference between the data are observed (Table 5). Fields for Early Gardar Depleted Mantle and a potential single mantle source (1.86 Ga) are given, with evolution trends for average Ketilidian Crust (1.9 Ga), Palaeoproterozoic (2.0) and late Archaean (2.5 Ga) mantle sources.

Fig. 7: Summary Geological Map of the Main Centres in the Motzfeldt – North Qôroq Volcanic System. Data are shown after reconstruction of fault movements (NSSQ – Narsarsuaq, NQ- North Qôroq, FDC – Flinks Dal Formation, MSC – Motzfeldt Sø Formation, GF – Geologfjeld Formation, NM – North Motzfeldt Centre). The present reconstruction correlates the rocks of the Motzfeldt Sø Formation South of the Flinks Dal fault (identified in a slightly darker yellow) as part of the North Qôroq centre.

Fig. 8: Schematic E-W cross Section through the Motzfeldt Volcanic System. The E-W section represents a horizontal line through the centre of Fig. 1, cutting rocks of the Flinks Dal and Motzfeldt Sø Centres. The 'Members' on the right hand side of the diagram refer to sedimentary units in the Eriksfjord succession inferred to have existed above current exposure levels. The unconformity between the Eriksfjord at Ketilidian basement is close to current exposure levels at Motzfeldt. The Flinks Dal Centre is interpreted as having punched through the unconformity between Ketilidian basement and the Eriksfjord such that current exposure of the FDC represents an equivalent to the MDC at depth.

TABLES

Centre	System Analysed	Age Estimate (Ma)	Reference
Motzfeldt	U-Pb on apatite	1350 ± 10	1
	Rb-Sr Whole Rock	1282 ± 30	2
	U-Pb on zircon	1275 ± 1	3
	U-Pb on zircon	1273 ± 6	4
Narsarsuaq	Rb-Sr Whole Rock	1282 ± 18	3
North Qôroq	Rb-Sr Whole Rock	1268 ± 60	2
North Motzfeldt	Rb-Sr Whole Rock	1258 ± 11	3
	U-Pb on zircon	1257 ± 7	3
	Rb-Sr Whole Rock	1226 ± 27	5

Table 1: Summary of Published Radiometric Age Data for rocks in the Motzfeldt – North Qôroq Volcanic System. References: 1 – Paslick *et al.* (1993), 2 – Blaxland *et al.* (1978), 3 – Salmon (2013), 4 – McCreath *et al.* (2012), 5- Finch *et al.* (2001).

	MSC				FDC				FDC raft
Wt.%	**23-2-2**	**29-7-2**	**66-1-1**		**87-4-6**	**87-16-1**	**91-9-2**		**84-3-1**
Na_2O	0.47	0.89	0.47		0.60	0.40	0.70		0.32
MgO	3.64	3.27	3.43		10.18	7.44	4.92		1.99
Al_2O_3	9.38	10.03	9.75		12.78	15.35	9.79		18.06
SiO_2	37.01	36.48	36.83		36.69	34.59	36.51		31.96
K_2O	9.11	9.83	10.51		9.89	9.93	9.63		10.59
CaO	0.00	0.00	0.00		0.03	0.00	0.03		1.97
TiO_2	3.29	5.03	5.33		3.93	3.17	2.68		2.64
MnO	0.35	0.74	0.68		1.23	1.38	1.31		0.38
FeO	32.69	30.96	29.26		19.55	23.83	30.26		26.97
F	0.98	1.09	1.07		2.46	1.51	0.46		1.16
Total	**95.94**	**98.34**	**96.26**		**97.35**	**97.59**	**95.83**		**96.04**
O≡F	0.41	0.46	0.45		1.04	0.63	0.19		0.49
Total	**95.53**	**97.88**	**95.81**		**96.31**	**96.96**	**95.83**		**95.55**
Fe/(Fe+Mg)	0.83	0.83	0.82		0.52	0.64	0.77		0.88
Al/(Al+Si)	0.08	0.25	0.14		0.15	0.11	0.07		0.08
Cations per 22 oxygen									
K	1.89	2.00	2.15		1.95	1.98	1.99		2.19
Na	0.15	0.28	0.15		0.18	0.12	0.22		0.10
Ca	0.00	0.00	0.00		0.00	0.00	0.00		0.34
Int site	**2.03**	**2.28**	**2.30**		**2.13**	**2.10**	**2.21**		**2.63**
Mg	0.88	0.78	0.82		2.34	1.73	1.19		0.48
Mn	0.05	0.10	0.09		0.16	0.18	0.18		0.05
Oct Fe	4.26	3.86	3.72		2.53	3.11	3.91		3.65
Oct Ti	0.40	0.60	0.64		0.46	0.37	0.33		0.32
Oct Al	0.00	0.00	0.00		0.04	0.28	0.00		0.70
Oct Total	**5.59**	**5.34**	**5.28**		**5.53**	**5.68**	**5.60**		**5.20**
Tet Al	1.83	1.92	1.88		2.33	2.60	1.90		2.82
Tet Fe	0.17	0.26	0.21		0.00	0.00	0.19		0.00
Si	6.00	5.81	5.91		5.67	5.40	5.91		5.18

Tet Total	**8.00**	**8.00**	**8.00**		**8.00**	**8.00**	**8.00**		**8.00**
F	0.50	0.55	0.54		1.20	0.74	0.23		0.60
Total Cations	**15.96**	**15.90**	**15.92**		**16.82**	**16.24**	**15.62**		**15.74**

Table 2: Representative EPMA analyses of biotite from the Motzfeldt centre. A full listing in given in supplementary information. All sample numbers have prefix GJM05. Tetrahedral site is filled by Si, Al and Fe in turn. Any excess Fe is allocated to the octahedral site. Oct = Octahedral, Tet = Tetrahedral.

Sample No.	Sample Description	$\delta^{13}C_{PDB}$	$\delta^{18}O_{SMOW}$
Motzfeldt Sø Formation			
GJM05/03	Altered syenite	-1.37	17.31
GJM05/16	Pegmatitic syenite	-2.31	19.18
GJM05/21	Altered syenite	-2.65	12.71
GJM05/24	Pyrochlore syenite	-3.31	15.89
GJM05/41	Altered microsyenite	-2.73	14.58
GJM05/59	Altered syenite	-3.43	14.82
GJM05/66	Altered syenite	-3.15	12.71
Flinks Dal Formation			
GJM06/98	Nepheline syenite	-3.84	12.96
GJM06/99	Nepheline syenite	-5.19	12.42
GJM06/110	Lujavrite	-3.80	13.96
GJM06/119	Microsyenite	-4.03	14.81
GJM06/125	Syenite	-6.60	13.54
GJM06/126	Vein calcite	-3.47	9.50
Flinks Dal Formation (Schönenberger & Markl, 2008)			
JS67	Vein calcite	-4.4	7.8
JS109	Calcite crystal in fluid inclusion	-3.9	8.1
JS181	Whole-rock powder (Flinks Dal formation)	-3.2	24.2
JS159	Whole-rock powder (Flinks Dal formation)	-2.2	21.9
JS164	Whole-rock powder (Flinks Dal formation)	-2.1	21.9
North Motzfeldt Diatremes			
AF/01/11	Carbonatite xenolith	-5.33	10.04
AF/01/12	Ferrocarbonatite sheet	-7.27	9.46
AF/01/13	Carbonatite xenolith	-4.20	13.80

Table 3: $\delta^{13}C$ and $\delta^{18}O$ composition of carbonates from the Motzfeldt region. Data include the Motzfeldt Sø Formation, Flinks Dal Formation and the North Motzfeldt Diatreme. Data from Schönenberger & Markl (2008) are added for comparison. Internal precision is typically 0.01 – 0.03 ‰ for $\delta^{13}C$ and 0.01-0.03 ‰ for $\delta^{18}O$ to 95% confidence.

Current Terms (present study)	Old
FDC – Porphyritic Syenite[1]	SM1, HY[4] and parts of SM4[2]
FDC – Nepheline Syenite[1]	Part of SM5[2]
FDC – Foyaite[1]	Part of SM5[2]
MSC, Geologfjeld[1]	SM1, SM3 and East Motzfeldt Syenite[2]
North Motzfeldt Centre[3]	Considered as part of Geologfjeld Formation[1] and as North Motzfeldt[2,3]
MSC – Peralkaline Microsyenite[1]	Microsyenites sheeting in the MSC[1] including SM6[4] and NM3[3]

Appendix Table 1: Comparison of Old and New Nomenclature for Rocks in the Motzfeldt Region. References: 1 – Tukianen (1985), 2 – Emeleus & Harry (1970), 3 – Finch *et al.* (2001), 4 – Jones (1990).

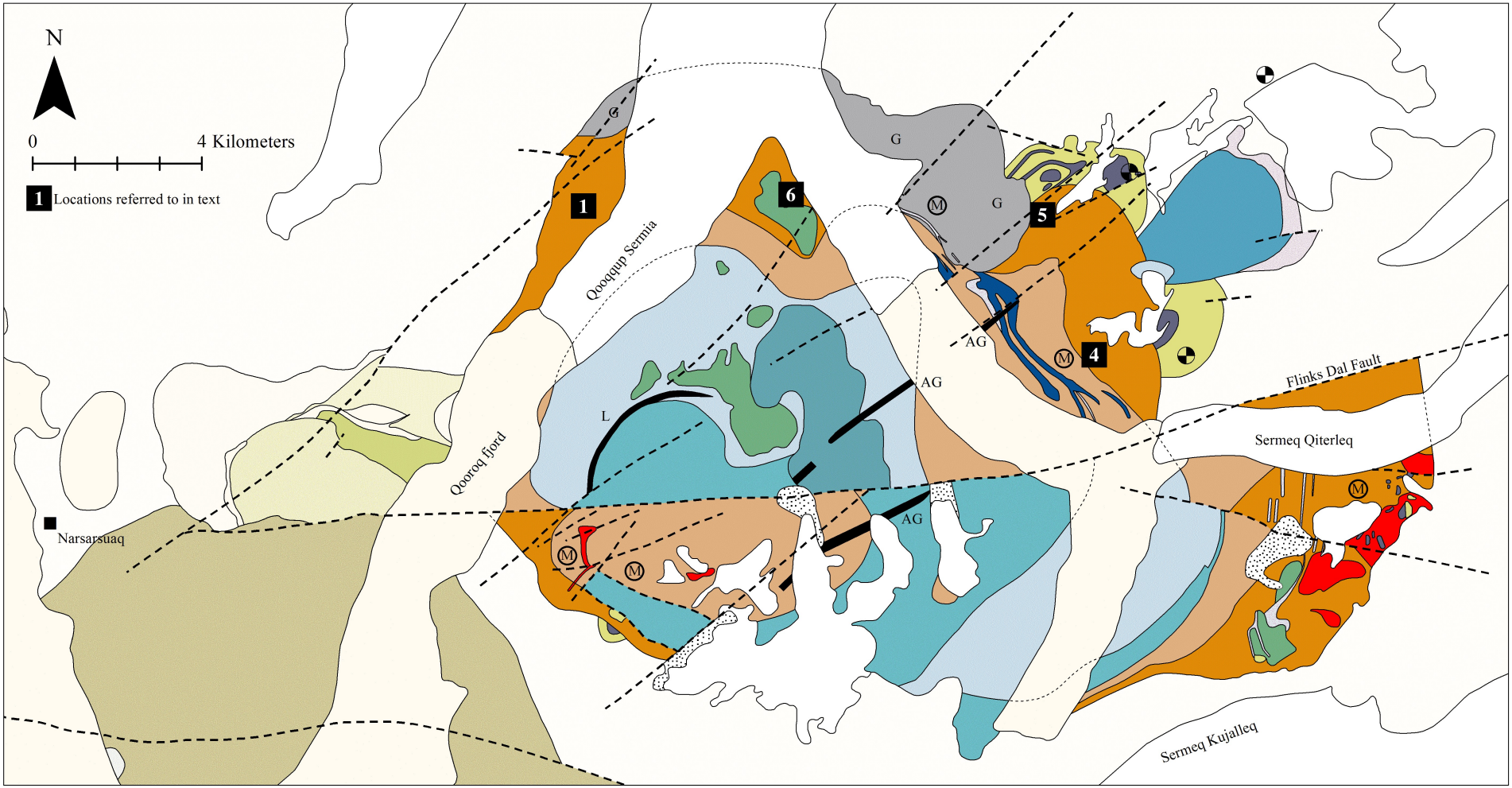

Motzfeldt:

Sheet intrusives and dykes
- L = Larvikite AG = Alkali gabbro
- Laminated alkali syenite
- Laminated porphyritic syenite

North Motzfeldt
- NM1
- NM2

Flinks Dal Formation
- Nepheline syenite
- Foyaite
- Porphyritic nepheline syenite

Motzfeldt Sø Formation
- Altered nepheline syenite
- Nepheline syenite
- Peralkaline microsyenite

Geologfjeld Formation
- G Syenite

Eriksfjord Formation
- Quartzite and sandstone
- Mafic extrusives
- Intermediate extrusives

North Qôroq: SN1A SN1B SN2 SN3 SN4A SN4B SN5

Other: Narsarsuaq Stock; Tunulliarfik; South Qôroq; Julianehåb batholith; Diatreme; (M) Significant microsyenite sheeting; Major fault; Moraine; Water and coastline

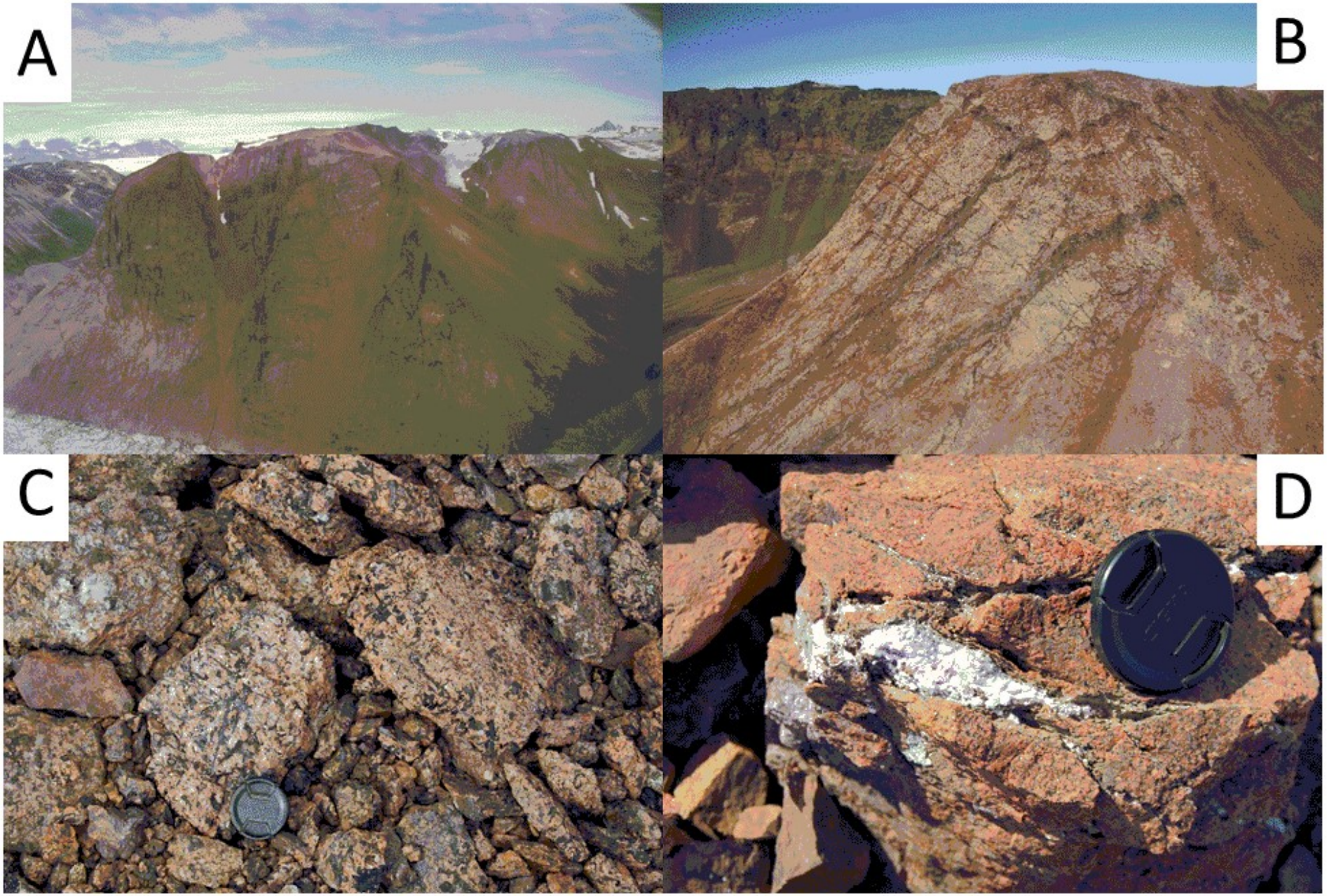
A
B
C
D

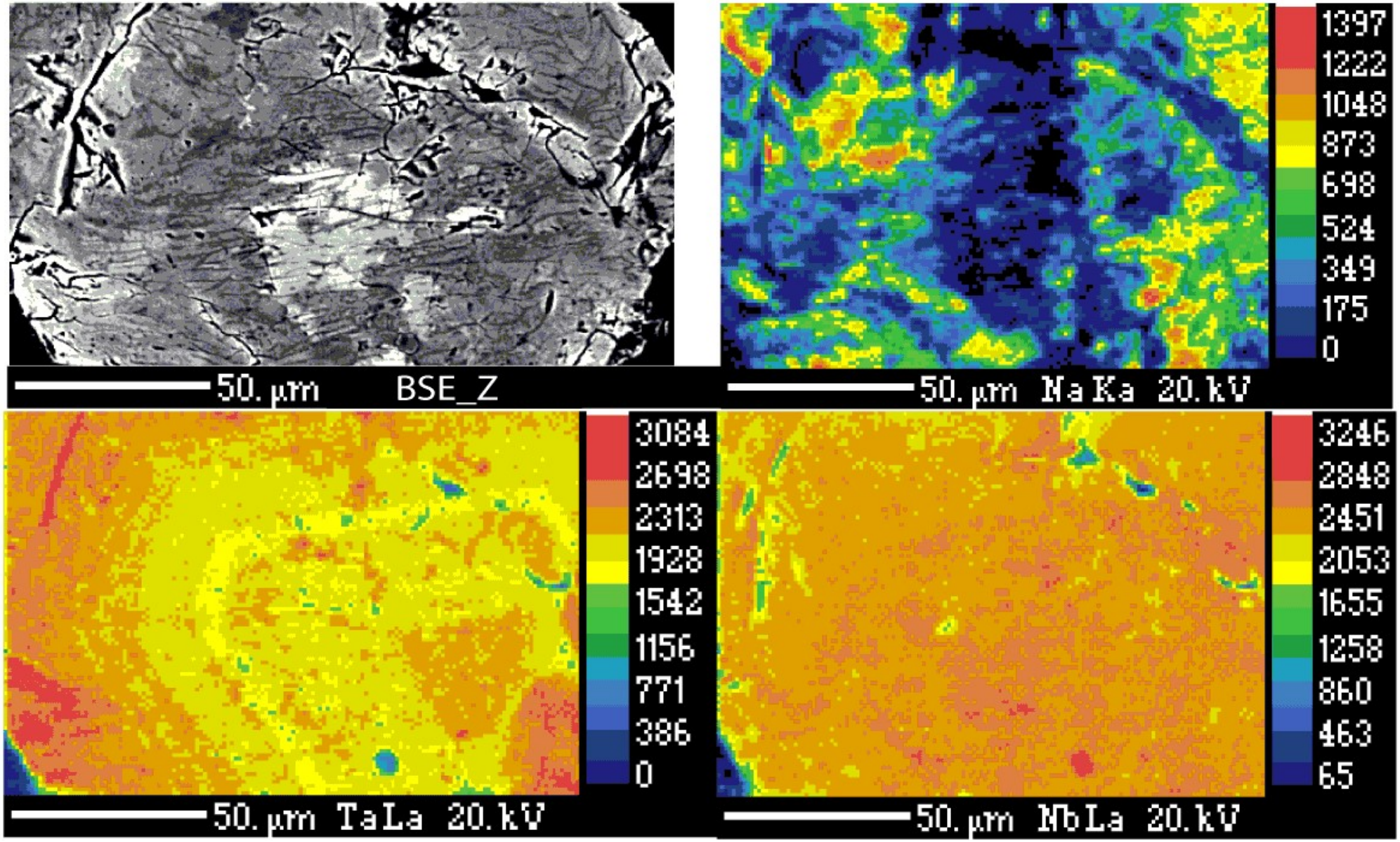
50. µm BSE_Z
50. µm Na Ka 20. kV
1397
1222
1048
873
698
524
349
175
0
50. µm Ta La 20. kV
3084
2698
2313
1928
1542
1156
771
386
0
50. µm Nb La 20. kV
3246
2848
2451
2053
1655
1258
860
463
65

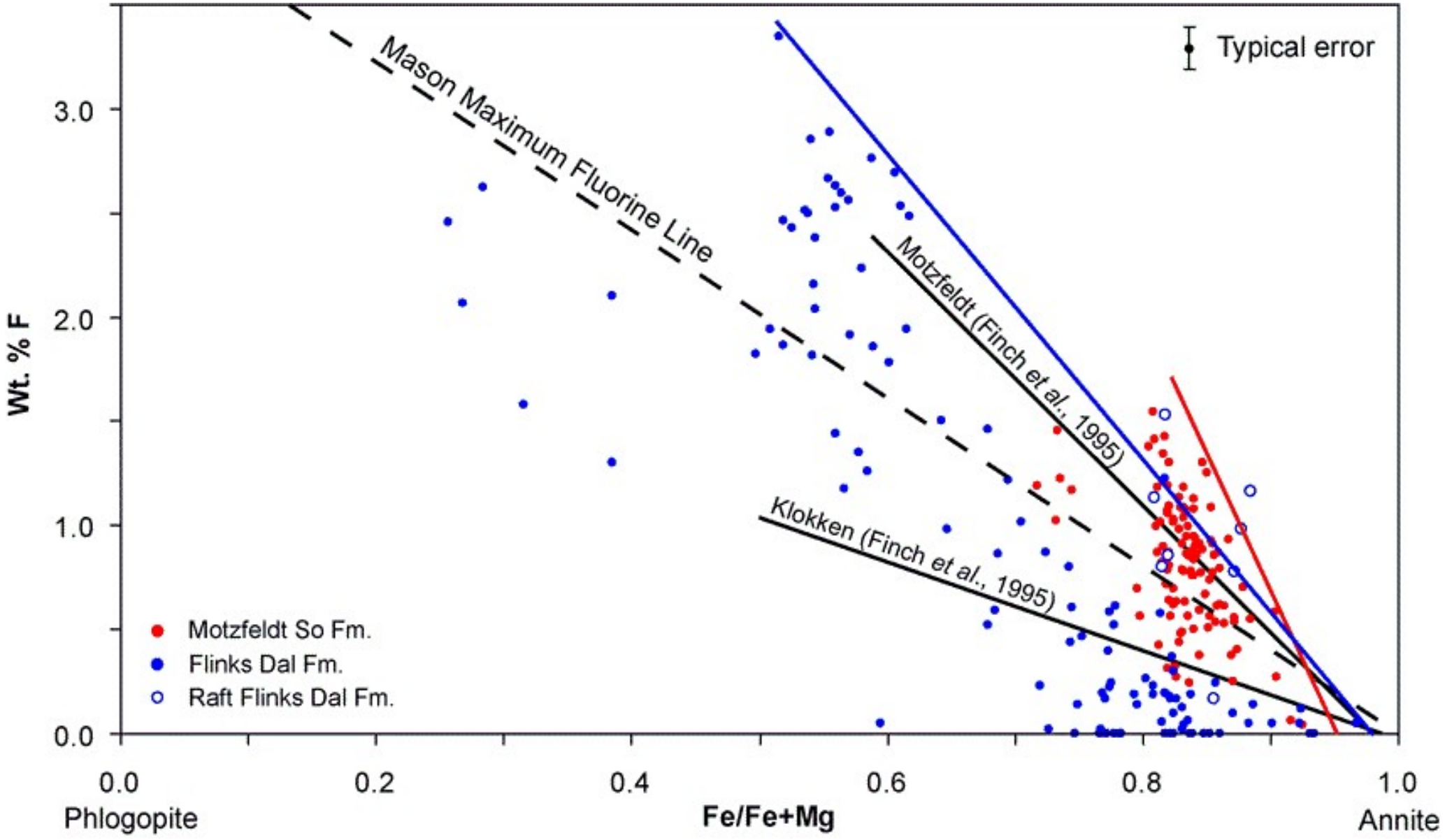
Typical error
Mason Maximum Fluorine Line
Motzfeldt (Finch et al., 1995)
Klokken (Finch et al., 1995)
Motzfeldt So Fm.
Flinks Dal Fm.
Raft Flinks Dal Fm.
Wt. % F
3.0
2.0
1.0
0.0
0.0
0.2
0.4
0.6
0.8
1.0
Phlogopite
Fe/Fe+Mg
Annite

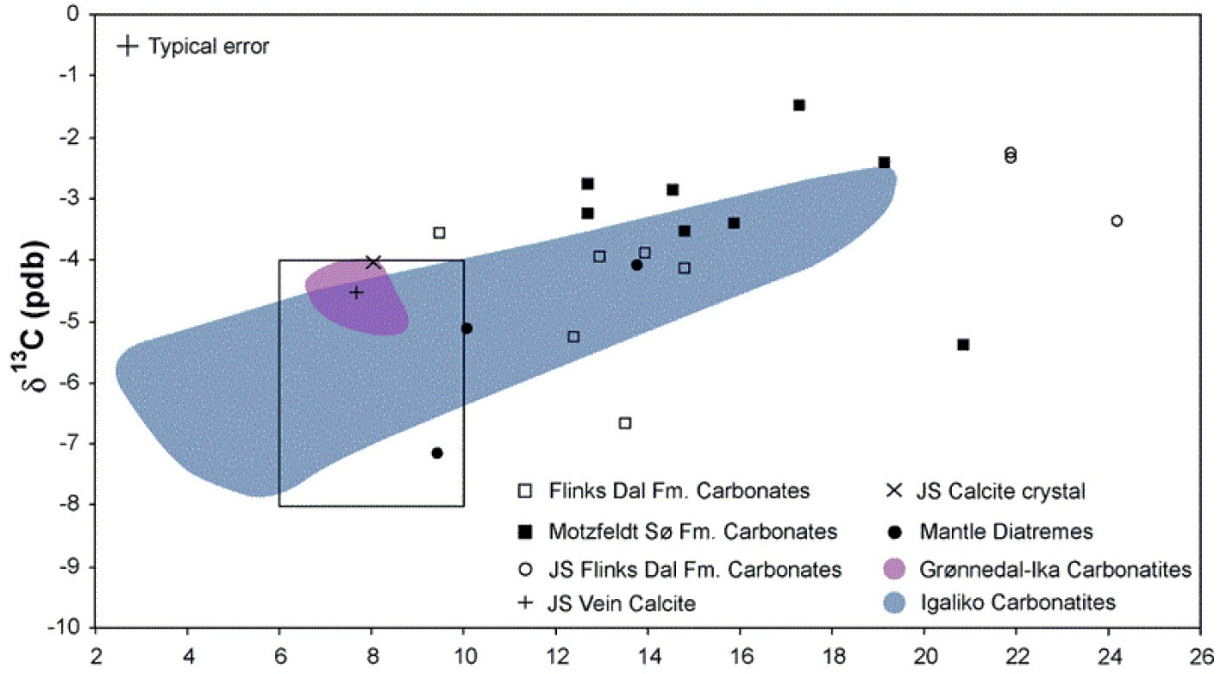
Typical error
δ13C (pdb)
Flinks Dal Fm. Carbonates
Motzfeldt Sø Fm. Carbonates
JS Flinks Dal Fm. Carbonates
JS Vein Calcite
JS Calcite crystal
Mantle Diatremes
Grønnedal-Ika Carbonatites
Igaliko Carbonatites

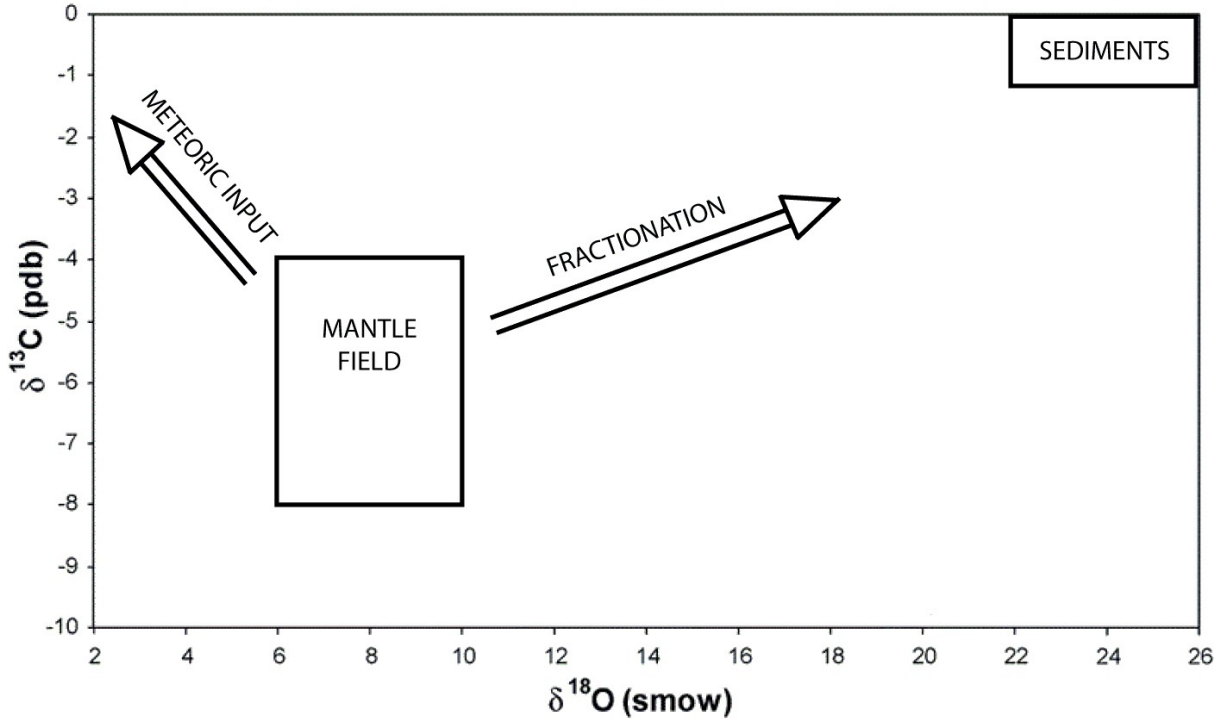
SEDIMENTS
METEORIC INPUT
FRACTIONATION
MANTLE FIELD
δ13C (pdb)
δ18O (smow)

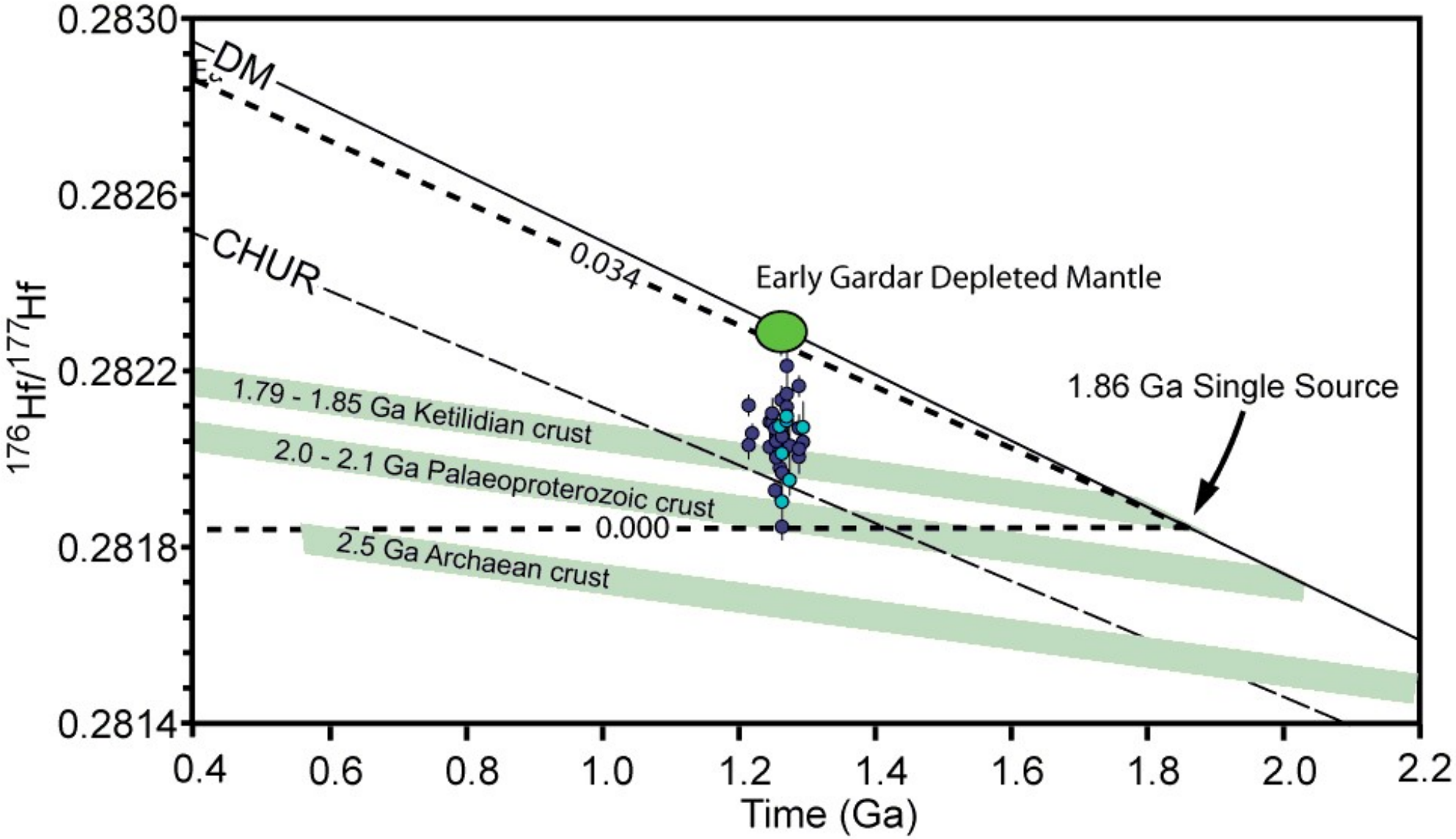
0.2830
0.2826
0.2822
0.2818
0.2814
$^{176}Hf/^{177}Hf$
DM
CHUR
0.034
0.000
Early Gardar Depleted Mantle
1.86 Ga Single Source
1.79 - 1.85 Ga Ketilidian crust
2.0 - 2.1 Ga Palaeoproterozoic crust
2.5 Ga Archaean crust
0.4
0.6
0.8
1.0
1.2
1.4
1.6
1.8
2.0
2.2
Time (Ga)

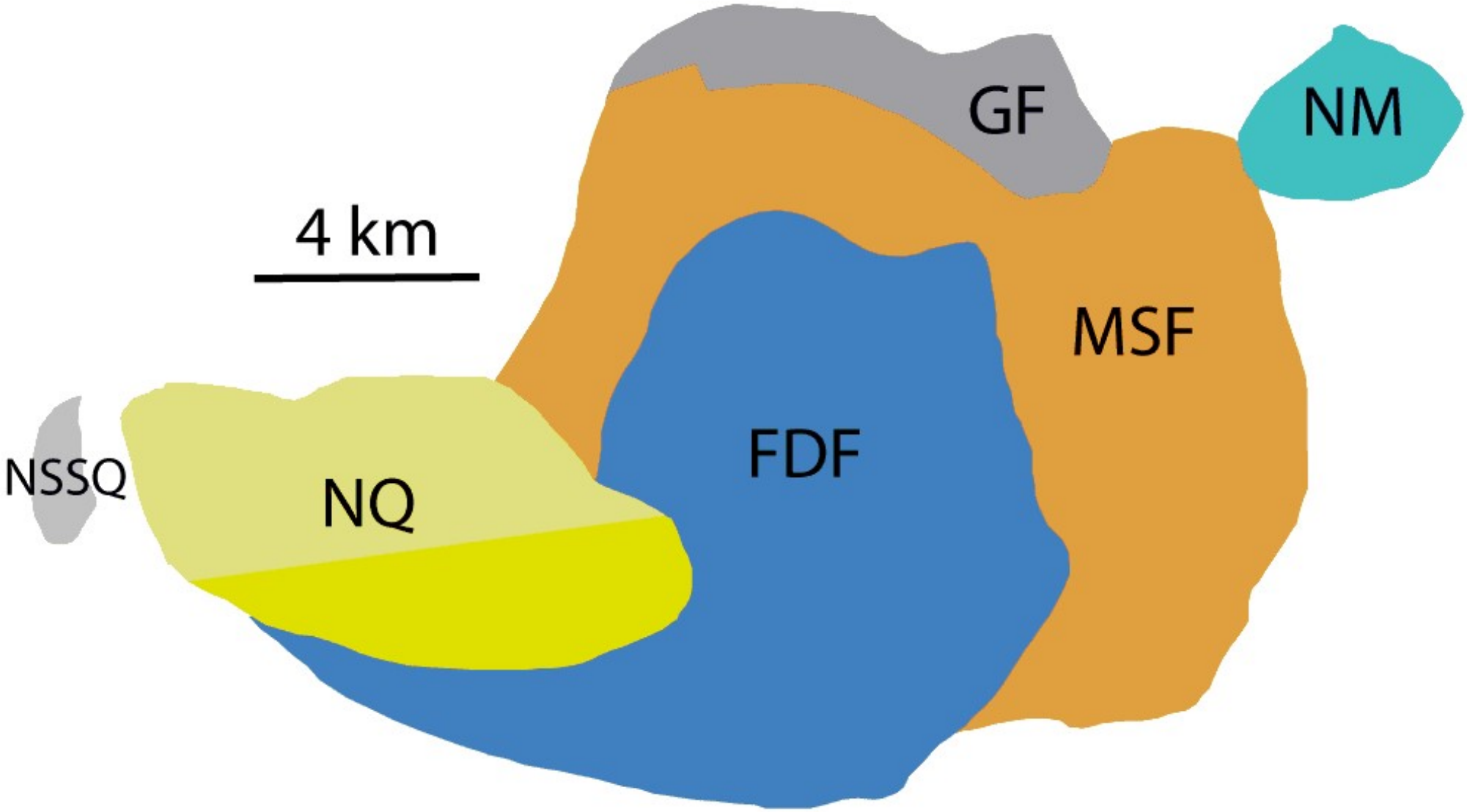
GF
NM
4 km
MSF
FDF
NSSQ
NQ

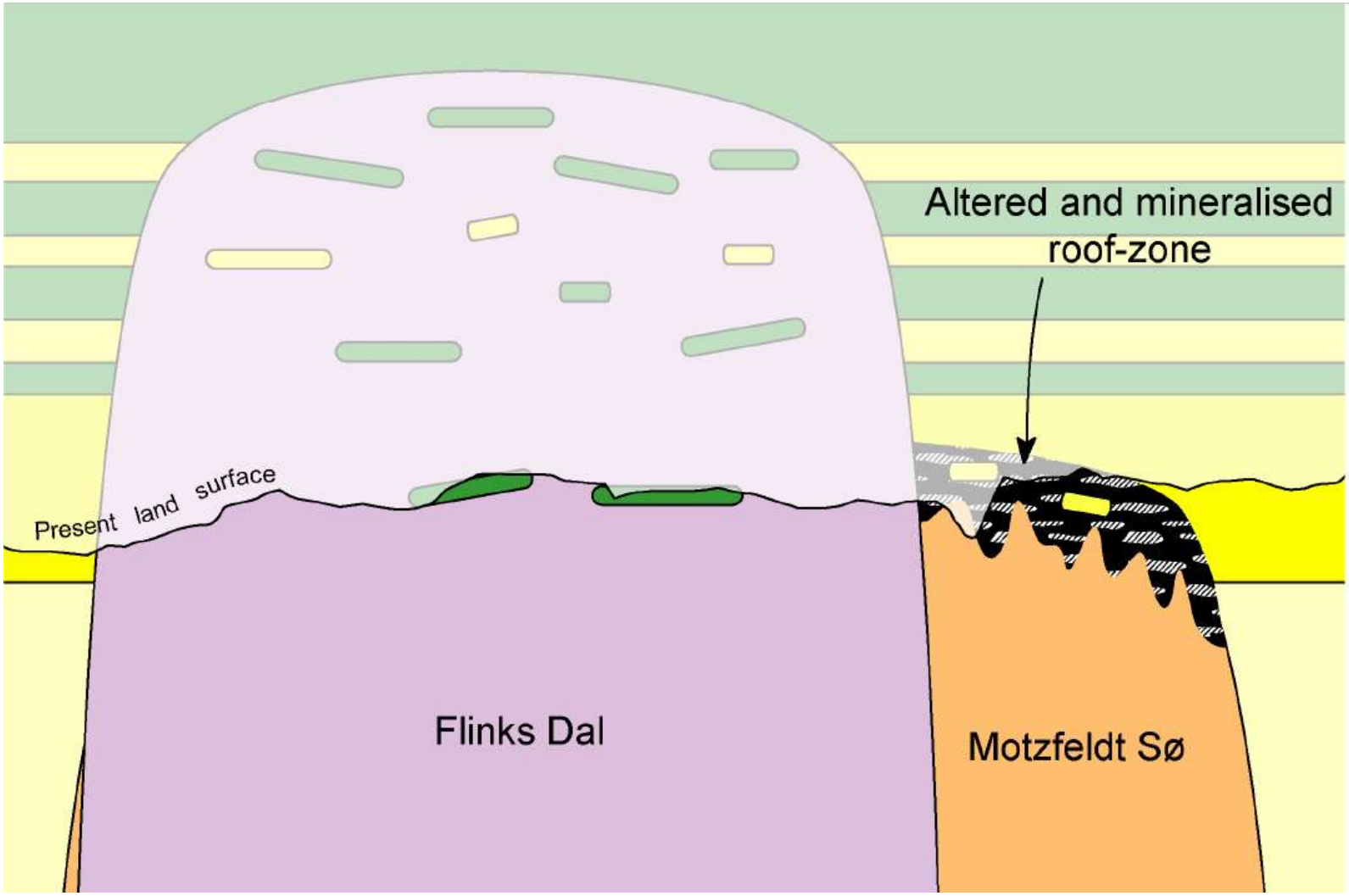

Ilímaussaq Member

Nunasarnaq Member

Ulukasik Member

Naujarssuit Member

Massartût Member

Majût Member

Julianehåb Granite